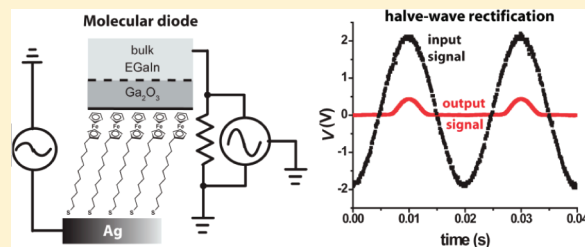


# A Molecular Half-Wave Rectifier

Christian A. Nijhuis,<sup>\*,†</sup> William F. Reus,<sup>‡</sup> Adam C. Siegel,<sup>‡</sup> and George M. Whitesides<sup>\*,‡</sup><sup>†</sup>Department of Chemistry, National University of Singapore, 3 Science Drive 3, Singapore 117543<sup>‡</sup>Department of Chemistry and Chemical Biology, Harvard University, Cambridge, Massachusetts 02138, United States

S Supporting Information

**ABSTRACT:** This paper describes the performance of junctions based on self-assembled monolayers (SAMs) as the functional element of a half-wave rectifier (a simple circuit that converts, or rectifies, an alternating current (AC) signal to a direct current (DC) signal). Junctions with SAMs of 11-(ferrocenyl)-1-undecanethiol or 11-(biferrocenyl)-1-undecanethiol on ultraflat, template-stripped Ag (Ag<sup>TS</sup>) bottom electrodes, and contacted by top electrodes of eutectic indium–gallium (EGaIn), rectified AC signals, while similar junctions based on SAMs of 1-undecanethiol—SAMs lacking the ferrocenyl terminal group—did not. SAMs in these AC circuits (operating at 50 Hz) remain stable over a larger window of applied bias than in DC circuits. AC measurements, therefore, can investigate charge transport in SAM-based junctions at magnitudes of bias inaccessible to DC measurements. For junctions with SAMs of alkanethiols, combining the results from AC and DC measurements identifies two regimes of bias with different mechanisms of charge transport: (i) low bias ( $|V| < 1.3$  V), at which direct tunneling dominates, and (ii) high bias ( $|V| > 1.3$  V), at which Fowler–Nordheim (FN) tunneling dominates. For junctions with SAMs terminated by Fc moieties, the transition to FN tunneling occurs at  $|V| \approx 2.0$  V. Furthermore, at sufficient forward bias ( $V > 0.5$  V), hopping makes a significant contribution to charge transport and occurs in series with direct tunneling ( $V \lesssim 2.0$  V) until FN tunneling activates ( $V \gtrsim 2.0$  V). Thus, for Fc-terminated SAMs at forward bias, three regimes are apparent: (i) direct tunneling ( $V = 0–0.5$  V), (ii) hopping plus direct tunneling ( $V \approx 0.5–2.0$  V), and (iii) FN tunneling ( $V \gtrsim 2.0$  V). Since hopping does not occur at reverse bias, only two regimes are present over the measured range of reverse bias. This difference in the mechanisms of charge transport at forward and reverse bias for junctions with Fc moieties resulted in large rectification ratios ( $R > 100$ ) and enabled half-wave rectification.



## INTRODUCTION

The field of molecular electronics applies the techniques and principles derived from studying inorganic electronic devices to investigating charge transport in organic molecules. While electrical engineers routinely use both alternating current (AC) and direct current (DC) to characterize traditional semiconductor devices, researchers in molecular electronics have, so far, relied mainly on DC measurements. Here, we show that using AC signals to investigate charge transport in self-assembled monolayers (SAMs) yields new information, including information that could not be obtained using DC signals alone, and provides a straightforward means of comparing the performance of molecular diodes against that of diodes based on traditional semiconductor technology.

This paper describes half-wave rectification of AC (50 Hz) signals by junctions based on SAMs. These junctions comprised SAMs of 11-(ferrocenyl)-1-undecanethiol (SC<sub>11</sub>Fc) or 11-(biferrocenyl)-1-undecanethiol (SC<sub>11</sub>Fc<sub>2</sub>), supported on template-stripped Ag (Ag<sup>TS</sup>) bottom electrodes, and contacted by top electrodes of eutectic indium–gallium (EGaIn, 75.5% Ga and 24.5% In by weight, 15.7 °C melting point, with a superficial layer of Ga<sub>2</sub>O<sub>3</sub>; Figure 1).<sup>1,2</sup> Similar junctions based on SAMs of 1-undecanethiol (SC<sub>10</sub>CH<sub>3</sub>)—SAMs lacking the ferrocenyl terminal group—did not rectify AC signals.

Previous experiments conducted using a DC bias of  $\pm 1.0$  V, and junctions based on SAMs of SC<sub>11</sub>Fc<sup>1</sup> and SC<sub>11</sub>Fc<sub>2</sub>,<sup>3</sup> yielded rectification ratios,  $R$  (defined by eq 1, where  $J$  is the current density (A/cm<sup>2</sup>) and  $V$  is the voltage (V)), of  $> 10^2$ . These high values of  $R$  make it possible to conduct physical-organic studies to determine the mechanism(s) of charge transport across these SAMs. We show that these systems—which are, in fact, “molecular diodes”—can substitute for conventional diodes in a simple circuit—a half-wave rectifier (Figure 1)—that converts an input AC signal into an output DC signal.<sup>4</sup>

$$R \equiv |J(-1.0 \text{ V})|/|J(+1.0 \text{ V})| \quad (1)$$

These molecular diodes, indeed, provide the basis for half-wave rectifiers. The circuits were stable for 30–40 min of operation, at a frequency of 50 Hz; this interval corresponds to more than  $10^5$  cycles. At low frequencies ( $\sim 1$  Hz) and at large input voltages ( $\sim 5$  V for SC<sub>11</sub>Fc and  $\sim 10$  V for SC<sub>11</sub>Fc<sub>2</sub>, see the Results and Discussion section), the junctions broke down more

Received: February 9, 2011

Published: August 15, 2011

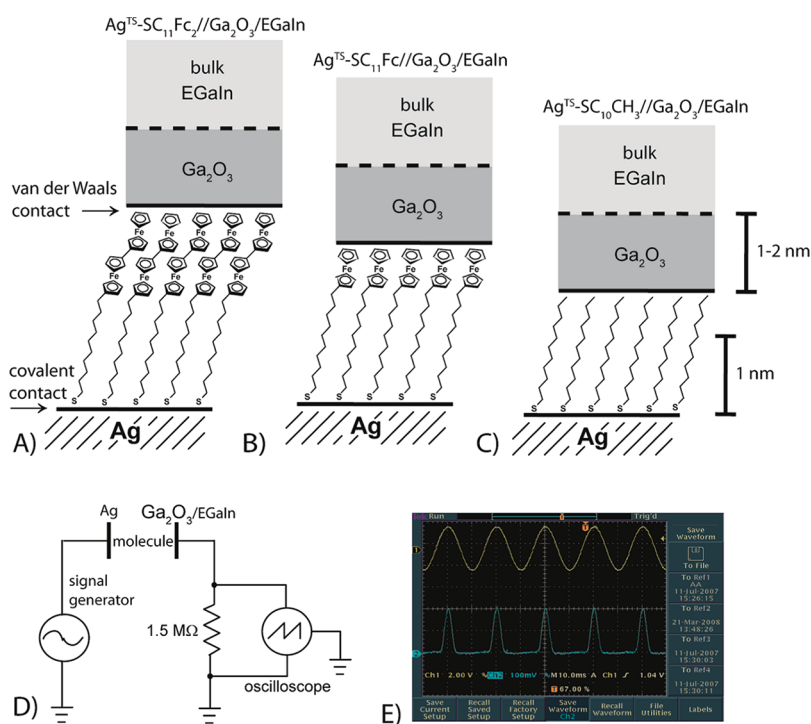


**Figure 1.** Schematic representations of the (A)  $\text{Ag}^{\text{TS}}\text{-SC}_{11}\text{Fc}_2//\text{Ga}_2\text{O}_3/\text{EGaIn}$ , (B)  $\text{Ag}^{\text{TS}}\text{-SC}_{11}\text{Fc}/\text{Ga}_2\text{O}_3/\text{EGaIn}$ , and (C)  $\text{Ag}^{\text{TS}}\text{-SC}_{10}\text{CH}_3//\text{Ga}_2\text{O}_3/\text{EGaIn}$  junctions, consisting of a  $\text{Ag}^{\text{TS}}$  bottom electrode and a cone-shaped  $\text{Ga}_2\text{O}_3/\text{EGaIn}$  top electrode. These diagrams represent “ideal” junctions. Real junctions have defects (see text for details). (D) The circuit with the molecular junction as the diode in series with a resistor ( $1.5\text{ M}\Omega$ ) and an AC signal generator. The circuit shows that the silver bottom electrode is biased. An oscilloscope simultaneously measures both  $V_{\text{in}}$  (the voltage applied by the signal generator) and  $V_{\text{out}}$  (the voltage across the resistor). (E) A screen image of the oscilloscope with a junction of the type of  $\text{Ag}^{\text{TS}}\text{-SC}_{11}\text{Fc}/\text{Ga}_2\text{O}_3/\text{EGaIn}$  in operation as a half-wave rectifier (the amplitude of sinusoidal input signal  $V_{\text{in}} = 2.0\text{ V}$  with a frequency of  $50\text{ Hz}$ ).

rapidly (typically after  $10^2\text{--}10^3$  cycles). In both circumstances the circuits failed by shorting across the SAM.

Using AC signals made it possible to study the mechanisms of charge transfer across the junctions as a function of potential over a much wider potential window (effective potentials across the junctions—see below for details—ranging from  $-5.0$  to  $2.2\text{ V}$  for  $\text{SC}_{11}\text{Fc}_2$ ,  $-4.0$  to  $2.2\text{ V}$  for  $\text{SC}_{11}\text{Fc}$ , and  $-1.5$  to  $1.6\text{ V}$  for  $\text{SC}_{11}$ ) than using a DC signal (typically limited to  $\pm 1.0\text{ V}$ ). Studying SAM-based junctions in these large potential windows allowed us to determine the breakdown voltages, and the practical limitations, of these molecular diodes, as well as to discriminate among tunneling, hopping, and field emission as mechanisms of charge transport.

Aviram and Ratner proposed in 1974 that molecules could act as diodes.<sup>5</sup> Since then, a variety of molecular diodes have been claimed,<sup>6–11</sup> including one example by us.<sup>12</sup> In general, reports of these diodes assume that rectification is a consequence of molecular structure (especially the group dipole of the structure). The difficulty in making meaningful measurements across SAMs has, however, made it practically impossible to correlate mechanisms of charge transport and rectification with the molecular and supramolecular structure of the SAM. Five characteristics of SAM-based junctions have complicated these measurements. (i) The molecular structures used in many studies have been unnecessarily complex.<sup>13–15</sup> (ii) The observed rectification ratios have often been close to unity (and perhaps statistically indistinguishable from unity),<sup>16–18</sup> including one example reported by us.<sup>12</sup> (iii) The reproducibility, yield, and operational lifetime of many of these systems have been low, or have not been reported.<sup>13</sup> (iv) Other asymmetries in the junction unrelated to

the molecular component—for example, electrodes of different materials, or junctions with two different types of contacts of the SAM with electrodes—may have contributed to rectification (without a molecular origin).<sup>11,19</sup> Cahen et al.<sup>20–22</sup> showed that their Si-alkyl/Hg-based junctions can give detailed information about the mechanisms of charge transport across these junctions, but detailed (and difficult) analysis is required in order to account for the Schottky barrier present at the Si-alkyl interface; in some cases, this Schottky barrier dominates charge transport through the junction. (v) Statistical analysis of the data involving rectification and studies of the stability of rectifying junctions have been largely absent in the literature;<sup>1,3,23,24</sup> it has, thus, been difficult to separate meaningful results from noise or artifacts.<sup>25–27</sup> Elsewhere, we have provided strong evidence that the rectification we reported was molecular in origin.<sup>1,3,28,32</sup> Here we show that rectifying junctions of the form  $\text{Ag}^{\text{TS}}\text{-SC}_{11}\text{Fc}/\text{Ga}_2\text{O}_3/\text{EGaIn}$  and  $\text{Ag}^{\text{TS}}\text{-SC}_{11}\text{Fc}_2//\text{Ga}_2\text{O}_3/\text{EGaIn}$  can be fabricated in good yields (70–90%), are stable over thousands of cycles, and give reproducible  $J(V)$  results.

The junction at one bias is the reference for the junction at the opposite bias, because the value of  $R$  is determined by dividing the current in the direction of bias by the current measured at the opposite direction (eq 1) across the same junction. Studying the rectification ratios, thus, eliminates many of the uncertainties related to contact resistances or contact areas (although some effects unrelated to the SAM, such as dipoles at interfaces between different materials, may also cause rectification).

AC measurements offer three advantages over DC measurements for investigating molecular rectification. (i) Using AC minimizes the formation of filaments by electromigration.<sup>29</sup>

Metal filaments can form in high electrical fields, especially when Ag electrodes are used, due to electromigration of atoms.<sup>30</sup> (ii) Using AC makes it possible to collect data rapidly: recording a  $J(V)$  curve by incrementally applying a DC bias usually takes several minutes, while recording the same curve with, for instance, an AC signal at 50 Hz takes 20 ms. (iii) Using AC makes it possible to incorporate a resistor in series with the molecular tunneling junction and effectively places an upper bound on the potential drop across the junction and protects against breakdown.

Rectifying SAM-based tunneling junctions have not been subjected to the sort of characterization in simple circuitry that is routine for diodes based on inorganic components, although such characterization is essential to determining the operational mechanisms and parameters—and thus the usefulness—of SAM-based rectifiers in electronic applications. This paper yields four important conclusions. (i) At high voltages across the SAM ( $V \gtrsim 2.0$  V), the SAM-based junctions have a mechanism of charge transport (field emission) that is different from the mechanism at low voltages (hopping and tunneling).<sup>31</sup> The half-wave rectifier (Figure 1D) incorporating these molecular diodes rectifies at input voltages less than 2.4 V but does not rectify at high input voltages in the range of 2.4–10 V (these voltages are specific to the circuit and depend on the choice of resistor). (ii) In operation, these molecular diodes have large internal resistances ( $\sim 10^6 \Omega$ ), suffer limited lifetimes (here 30–40 min in operation at 50 Hz), and break down outside of a relatively small window of applied bias ( $-5.0$  to  $2.2$  V). Reporting only values of  $R$  for a molecular diode is insufficient to characterize its performance and establish its practical usefulness. (iii) The breakdown voltages of the diodes determined using the AC method are a factor of 2 larger than those determined by DC methods. This result implies that AC signals, indeed, reduce the formation of metal filaments, or other possible side reactions, inside the SAM-based junctions. Thus, the method described in this paper provides both information about the practical utility and limitations of SAM-based diodes, and fundamental information about the mechanisms of charge transport. (iv) The properties of these systems suggest them as excellent models with which to study the mechanisms of charge transport in organic matter, but do not show (so far) properties that indicate a potential advantage over conventional inorganic rectifiers in practical applications.

## ■ PRIOR WORK

**Junctions with Top Electrodes of Cone-Shaped Tips of  $\text{Ga}_2\text{O}_3/\text{EGaIn}$ .** We have previously described the fabrication of junctions of the form  $\text{Ag}^{\text{TS}}\text{-SAM//Ga}_2\text{O}_3/\text{EGaIn}$  with SAMs of  $n$ -alkanethiolates<sup>2</sup> and ferrocene-terminated alkanethiolates.<sup>1</sup> This method produces stable, reproducible molecular tunneling junctions with bottom electrodes of template-stripped Ag ( $\text{Ag}^{\text{TS}}$ ) and cone-shaped top electrodes of  $\text{Ga}_2\text{O}_3/\text{EGaIn}$  suspended from a syringe. Although this system still requires an experienced operator, and substantial attention to procedure and experimental detail, it can generate data with good reproducibility.<sup>1,3</sup> This reproducibility, combined with the stability of these molecular junctions (they can withstand many cycles of applied bias, as well as small mechanical disturbances), enables their use in physical-organic studies measuring the effect of the composition and structure of the SAM on charge transport.

**The Influence of the Layer of  $\text{Ga}_2\text{O}_3$  on the Characteristics of the Junctions.** We have studied the influence of the layer of

$\text{Ga}_2\text{O}_3$  on the  $J(V)$  characteristics of these SAM-based junctions. We concluded that the layer of  $\text{Ga}_2\text{O}_3$  has a resistance that is at least 3–4 orders of magnitude smaller than that of a SAM of  $\text{SC}_{10}\text{CH}_3$ .<sup>1,3,32</sup> We also found that the mechanism of charge transport across this layer is thermally activated.<sup>32</sup> We believe that the influence of the layer of  $\text{Ga}_2\text{O}_3$  on the electrical properties of these SAM-based junctions is insignificant: the electrical properties of these junctions are dominated by the chemical and supramolecular structure of the SAM.

Detailed studies by secondary ion mass spectroscopy (ToF SIMS), scanning electron microscopy (SEM), and angle-resolved X-ray photoelectron spectroscopy (ARXPS) indicated that the layer of gallium oxides (i) has an average thickness of 0.7 nm, (ii) has substantial roughness, (iii) is mainly composed of  $\text{Ga}_2\text{O}_3$ , though  $\text{Ga}_2\text{O}$  and  $\text{In}_2\text{O}_3$  are also present, and (iv) supports a discontinuous layer of adsorbed organic material (the fraction of the surface covered by this layer, and the chemical composition of the layer, may depend on the ambient conditions).<sup>33</sup> This organic layer is probably the least understood component of our system, and we are working to quantify or eliminate it,<sup>34</sup> but it has not prevented us from obtaining meaningful results in controlled physical-organic studies.

Using inverted optical microscopy, we observed that the visible contact area between the cone-shaped tip of  $\text{Ga}_2\text{O}_3/\text{EGaIn}$  and the SAM is  $\sim 25\%$  of the measured contact area.<sup>3,32,35</sup> The (presumably normally distributed) uncertainty of estimating the actual contact area is, at present, not a dominant (and in many systems not even significant) component of the log-normally distributed uncertainty that we observe in  $J(V)$  measurements.

We measured the electrical properties of the layer of  $\text{Ga}_2\text{O}_3$  and concluded that, in a typical junction, the resistance of this layer is at least 4 orders of magnitude less than that of a SAM of  $\text{SC}_{10}\text{CH}_3$ .<sup>3,32,35</sup> Hence, we do not believe that the electrical properties of the layer of  $\text{Ga}_2\text{O}_3$  significantly affect charge transport through SAM-based junctions. The low resistance of the layer of  $\text{Ga}_2\text{O}_3$  fits with the observation that this layer contains many defects, which may dope the material and increase its conductivity. Theoretically, a defect-free thin film of  $\text{Ga}_2\text{O}_3$  should be insulating.<sup>36</sup>

**Molecular Rectification by SAMs of  $\text{SC}_{11}\text{Fc}$ .** We found that two characteristics of the SAMs of  $\text{SC}_{11}\text{Fc}$  inside the junctions cause the large observed rectification ratios ( $R \approx 1.0 \times 10^2$ , measured at  $\pm 1.0$  V, DC measurements): (i) the potential drop across the SAM is nonuniform because the SAM is asymmetric,<sup>3</sup> and (ii) the mechanism of charge transport changes from tunneling to hopping in only one direction of bias, and not in the other.<sup>32</sup>

The SAMs of  $\text{SC}_{11}\text{Fc}$  rectify only when the Fc moiety is located asymmetrically in the SAM: that is, the Fc moiety must be in close spatial proximity to one of the electrodes. In our junctions, the Fc moiety is in van der Waals contact with the  $\text{Ga}_2\text{O}_3/\text{EGaIn}$  top electrode but is separated from the  $\text{Ag}^{\text{TS}}$  bottom electrode by the  $\text{C}_{11}$  alkyl chain.<sup>3</sup> Consequently, the HOMO of the Fc moiety follows the Fermi level of the top electrode. The HOMO of the Fc is energetically accessible only when it overlaps with both Fermi levels, which, in our case, is possible only at negative bias and not at positive bias. Figure 2 shows the energy level diagrams for the  $\text{Ag}^{\text{TS}}\text{-SC}_{11}\text{Fc/Ga}_2\text{O}_3/\text{EGaIn}$  junctions at a bias of  $-1.0$  and  $1.0$  V.

At sufficient negative bias, the HOMO of the Fc can participate in charge transport, and the potential drops mainly across the  $\text{C}_{11}$  alkyl chain. At positive bias, the HOMO of the Fc cannot



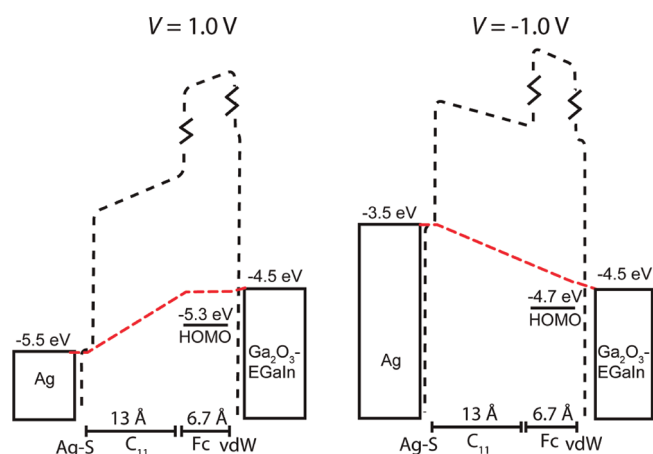


**Figure 2.** Schematic representation of the energy level diagrams (with respect to vacuum) of the Ag<sup>TS</sup>-SC<sub>11</sub>Fc//Ga<sub>2</sub>O<sub>3</sub>/EGaIn junctions at 1.0 V (left) and -1.0 V (right) bias. Ag-S denotes the covalent bond between the thiol and the Ag<sup>TS</sup> substrate, C<sub>11</sub> denotes the alkyl chain, Fc denotes ferrocene, and vdW denotes the van der Waals contact of the SAM with the Ga<sub>2</sub>O<sub>3</sub>/EGaIn. The dotted lines qualitatively represent the lowest unoccupied molecular orbitals for the alkyl chain (approximately -2.6 to -2.9 eV)<sup>37</sup> and the Fc moiety (approximately -0.4 eV).<sup>38,39</sup> A detailed explanation of these energy-level diagrams, including justifications for the estimated values of the Fc HOMO at forward and reverse bias, can be found in our previous work.<sup>3</sup>

participate in charge transport, and the potential drops more or less equally along both the C<sub>11</sub> and Fc moieties. The difference in the profile of the potential across the junction, at positive and negative bias, causes rectification.<sup>3</sup>

Measurement of  $J(V)$  as a function of temperature indicated that, at negative bias, when the HOMO of the Fc participates in charge transport, the mechanism of charge transport changes from tunneling (which is independent of  $T$ ) to hopping (which is dependent on  $T$ ), while at positive bias, when the HOMO cannot participate in charge transport, the mechanism of charge transport is tunneling for all measured  $T$ .<sup>32</sup>

This change in the mechanism of charge transport effectively reduces the width of the tunneling barrier in one direction of bias (but not the other) from ~2.0 nm (the entire length of the SC<sub>11</sub>Fc molecule) to ~1.3 nm (the length of the SC<sub>11</sub> alkyl chain). Charges must, therefore, tunnel across a much wider barrier at reverse bias than at forward bias. This change in the width of the tunneling barrier results in the large observed rectification ratios of  $1.0 \times 10^2$ .

**Other Junctions with SC<sub>11</sub>Fc.** Zandvliet et al.<sup>40</sup> showed, using a tungsten STM tip as a top electrode, that molecules of SC<sub>11</sub>Fc inserted in SAMs of SC<sub>11</sub> on Au rectify currents with a rectification ratio of about 10. The lower values of  $R$  observed in their experiment could be caused by a lower density of SC<sub>11</sub>Fc in their SAM, and/or the presence of an additional tunneling barrier—the vacuum gap between the SAM and the STM tip—in their junctions. A second study reported a rectification ratio of 20 by contacting a monolayer of SC<sub>6</sub>Fc on Au with a Au-STM tip.<sup>41</sup>

We reported that tunneling junctions of SAMs of SC<sub>11</sub>Fc on Ag<sup>TS</sup> electrodes contacted with template-stripped Au foil (with a thickness of 50 nm) rectified currents with values of  $R$  of 10–100.<sup>3</sup> Although these junctions were not stable enough to measure more than one to five traces, did not generate statistically large numbers of data, and gave low yields in working devices (<10%), they showed

that rectification in these SAMs is caused by the chemical structure of the SAM, and not by any of the other asymmetries in the junctions of Ag<sup>TS</sup>-SC<sub>11</sub>Fc//Ga<sub>2</sub>O<sub>3</sub>/EGaIn.

**Mechanisms of Charge Transport across SAMs.** Three different mechanisms of charge transport across SAMs have been experimentally observed in SAM-based junctions: (i) tunneling (both coherent, in which the phase of the tunneling charge is preserved, and incoherent, in which scattering changes the phase), (ii) hopping, and (iii) Fowler–Nordheim (FN) tunneling.<sup>31</sup> Frisbie et al.<sup>42</sup> showed that the mechanism of charge transport in junctions with conjugated molecular wires changes from tunneling to hopping as the molecular length increases. Using a conducting tip of an atomic force microscope as the top contact, they measured the conductivities of a series of oligophenyleneimines (OPI), with lengths ranging from 1.5 to 7.3 nm, immobilized on gold bottom electrodes. Their studies revealed that the dominant mechanism of charge transport across these junctions was tunneling for molecular wires shorter than ~4 nm, but the mechanism changed to hopping for molecular wires exceeding ~4 nm in length. Beebe et al.<sup>43,44</sup> showed that FN tunneling is important in SAM-based tunneling junctions above a critical voltage, the so-called transition voltage ( $V_{\text{trans}}$ ). Above the transition voltage, which depends on the shape and height of the tunneling barrier, the mechanism of charge transport changes from tunneling to FN tunneling.

#### Theory of the Mechanisms of Charge Transport: Tunneling.

There is a broad consensus that the mechanism of charge transport across SAMs of *n*-alkanethiolates is coherent tunneling.<sup>45,46</sup> The chemical and supramolecular structure defines the width of the tunneling barrier, and the HOMO and LUMO levels define the height of this barrier. The mechanism of charge transport across these tunneling junctions is usually interpreted in terms of a model proposed by Simmons to describe tunneling through an inorganic insulator.<sup>47,48</sup> The model uses a generalized tunneling barrier—two metal electrodes separated by an insulator—with a trapezoidal shape under applied bias. As Simmons made clear, this model does not account for the image potential induced in the barrier by the electrodes. The image potential effectively rounds off the corners of the barrier and reduces its effective height and, consequently, increases the probability of tunneling. The Simmons equation also neglects a number of other, possibly relevant, features of SAMs, particularly their anisotropic structure and the dissimilarity of molecular orbitals to the electronic bands in inorganic materials.

A simple form of the Simmons equation (eq 2) describes this barrier, where  $J_0$  (A/cm<sup>2</sup>) is a constant and depends on the system and includes contact resistance,  $d$  (Å) is the width of the tunneling barrier, and the  $\beta$  (Å<sup>-1</sup>) is the decay constant. Many groups have reported that tunneling through a SAM is more efficient ( $\beta = 0.80$  Å<sup>-1</sup>) than through space ( $\beta = 2.9$  Å<sup>-1</sup>) for a vacuum gap between two metals with work functions of 5 eV.<sup>45</sup> The difference between the values of  $\beta$  for vacuum and “insulating” organic matter is explained by superexchange tunneling.<sup>49</sup> The orbitals of the organic molecule reduce the potential barrier to charge carriers within the junction, and increase the probability of tunneling. This effect makes “through-bond” tunneling more efficient than “through-space” tunneling.<sup>50</sup> No current theory, however, quantitatively predicts a value for  $\beta = 0.80$  Å<sup>-1</sup>.

$$J = J_0 e^{-\beta d} \quad (2)$$

**Theory of the Mechanisms of Charge Transport: Fowler–Nordheim Tunneling.** Fowler–Nordheim tunneling, or field

emission, is the emission of electrons under the influence of large electric fields from a metal, or semiconductor, into a vacuum, or dielectric. In SAM-based junctions, large electric fields (for example, 1.0 V bias across a junction of 1 nm results in an electric field of 1.0 GV/m) can cause emission of electrons from the electrodes to the SAM. Thus, the mechanism of charge transport changes from tunneling to FN tunneling with increasing electric field. Beebe et al.<sup>43,44</sup> inferred that the Simmons theory can be used to determine the potential at which the mechanism of charge transport changes from tunneling to field emission, or FN tunneling, when the barrier shape changes from rectangular to triangular when bias is applied.

Equation 3 gives the original form of the Simmons equation ( $A$  is the junction area,  $d$  the barrier width,  $m_e$  the mass of the electron,  $\Phi$  the barrier height, and  $q$  the electronic charge):

$$I = \frac{qA}{4\pi^2 \hbar^2 d^2} \left\{ \left( \phi - \frac{qV}{2} \right) \exp \left( -\frac{2d\sqrt{2m_e}}{\hbar} \sqrt{\phi - \frac{qV}{2}} \right) - \left( \phi + \frac{qV}{2} \right) \exp \left( -\frac{2d\sqrt{2m_e}}{\hbar} \sqrt{\phi + \frac{qV}{2}} \right) \right\} \quad (3)$$

In molecular junctions the barrier width is defined by the molecular length, and the barrier height corresponds to the energy offset between the Fermi levels of the electrodes and the nearest molecular orbital, i.e., the LUMO levels of the alkyl group and the Fc or Fc<sub>2</sub> moiety. Beebe et al.<sup>43,44</sup> described a method to estimate this barrier height. Near zero bias, the barrier shape is rectangular, and eq 3 reduces to eq 4.

$$I \propto V \exp \left( -\frac{2d\sqrt{2m_e}\phi}{\hbar} \right) \quad (4)$$

In contrast, at the high-bias limit, the barrier shape changes from rectangular to triangular, and the Simmons-like behavior is replaced by a FN dependence, which describes tunneling of electrons (holes) through a triangular barrier into the conduction (valence) band of an insulator or semiconductor, and subsequent field emission (eq 5).

$$I \propto V^2 \exp \left( -\frac{4d\sqrt{2m_e}\phi^3}{3\hbar qV} \right) \quad (5)$$

Linearization of eq 5 gives eq 6.<sup>43,44</sup>

$$\ln \left( \frac{I}{V^2} \right) \propto -\frac{4d\sqrt{2m_e}\phi^3}{3\hbar q} \left( \frac{1}{V} \right) \quad (6)$$

According to eq 6, the slope of a plot of  $\ln(I/V^2)$  versus  $1/V$  gives an estimate of the barrier height. In the low-bias limit, a plot of  $\ln(I/V^2)$  versus  $1/V$  can be described by eq 7.<sup>43,44</sup>

$$\ln \left( \frac{I}{V^2} \right) \propto -\ln \left( \frac{1}{V} \right) - \frac{2d\sqrt{2m_e}\phi}{\hbar} \quad (7)$$

Equations 6 and 7 predict that a plot of  $\ln(I/V^2)$  versus  $1/V$  will show a transition from logarithmic growth to linear decay.<sup>43,44</sup> Beebe et al.<sup>43,44</sup> argued that a transition of the mechanism of charge transport from tunneling (logarithmic) to field emission (linear) would result in an inflection point in a plot of  $\ln(I/V^2)$  versus  $1/V$ . The potential at which this transition occurs is the so-called transition potential,  $V_{\text{trans}}$ . The Simmons equation does not take into account the potential drops across

the contacts, or the image potentials, and the effective mass of the electrons crossing the junction may be different from the mass of an electron. Thus, a plot of  $\ln(I/V^2)$  versus  $1/V$  only provides a first-order estimate of the barrier heights of the tunneling junctions.

## EXPERIMENTAL DESIGN

We reported the procedure for the analysis of the  $J(V)$  data obtained by DC methods before, but we give a short description here.<sup>1,3,32</sup> Plotting histograms of all values of  $|J|$  measured for a certain potential established that  $|J|$  is log-normally distributed; i.e.,  $\log(|J|)$  is normally distributed. A log-normal distribution results from a randomly distributed variable whose logarithm is normally distributed. Thus, if variable  $Y$  is normally distributed, and  $X$  depends exponentially on  $Y$ , i.e.,  $X \propto e^Y$ , then  $\log X$  is normally distributed and  $X$  is log-normally distributed. The value of  $J$  depends exponentially on the distance  $d$  between the top and bottom electrodes (eq 2). We believe that  $d$  is normally distributed; this distribution results in a log-normal distribution of the values of  $J$ .

We fitted histograms of  $\log(|J|)$  with Gaussian functions, from which we determined the log-mean and log-standard deviation of  $|J|$  at all measured potentials. These values were used to construct the average  $J(V)$  curves. We performed a similar analysis to determine the values for  $R$ .<sup>1,3,32</sup>

We used AC signals with a frequency of 50 Hz with amplitude ranging from 0.80 to 10.0 V. We did not observe measurable output signals for input signals with an amplitude of <0.80 V, and the junctions shorted faster (after  $10^2$ – $10^3$  cycles) with input signals of >5.0–10.0 V.

We used a simple breadboard to connect the molecular junctions to the wave generator, oscilloscope, and resistor. This simple circuit was not free of capacitive currents; these were significant at frequencies of the input signal of >100 Hz. We found that at low frequencies (<10 Hz) the junctions tended to short more rapidly than at relatively high frequencies (>10 Hz). We chose to use a frequency of 50 Hz to minimize capacitive currents without compromising the lifetimes of the junctions during the experiments.

We used a large resistor (1.5 M $\Omega$ ) in series with the junction to minimize the currents across the junctions during the experiments; the purpose of this resistor was to limit the current through the tunneling junctions for the AC input signals with large amplitudes close to the breakdown voltages of the junction (2–10 V) when the resistance of the tunneling junction decreases significantly.

We used junctions of the form of Ag<sup>TS</sup>-SAM//Ga<sub>2</sub>O<sub>3</sub>/EGaIn for three reasons. (i) The template-stripped bottom electrodes are ultraflat. These electrodes have a surface roughness that is 5 times lower than that of bottom electrodes obtained from direct metal deposition techniques.<sup>51</sup> (ii) The SAMs of SC<sub>11</sub>Fc give rectification ratios of 2 orders of magnitude.<sup>1,3,32</sup> These high rectification ratios make it possible to conduct physical-organic studies of charge transport. (iii) The Ga<sub>2</sub>O<sub>3</sub>/EGaIn top electrodes form stable contacts with the SAMs.<sup>1–3,32</sup> This stability makes it possible to observe the electrical characteristics of the junctions over the course of several hours.

## RESULTS AND DISCUSSION

### Current Density Measurements of the Tunneling Junctions.

Figure 1 shows idealized schematic representations of the Ag<sup>TS</sup>-SC<sub>11</sub>Fc<sub>2</sub>//Ga<sub>2</sub>O<sub>3</sub>/EGaIn, Ag<sup>TS</sup>-SC<sub>11</sub>Fc//Ga<sub>2</sub>O<sub>3</sub>/EGaIn, and Ag<sup>TS</sup>-SC<sub>10</sub>CH<sub>3</sub>//Ga<sub>2</sub>O<sub>3</sub>/EGaIn junctions. In reality, SAMs in these junctions have defects due to pinholes, step edges, etch pitches, phase domains, grains, grain boundaries, and impurities.<sup>52</sup> We have described the  $J(V)$  characteristics obtained with DC measurements, and detailed discussions of the possible defects in our tunneling junctions and their influence on the

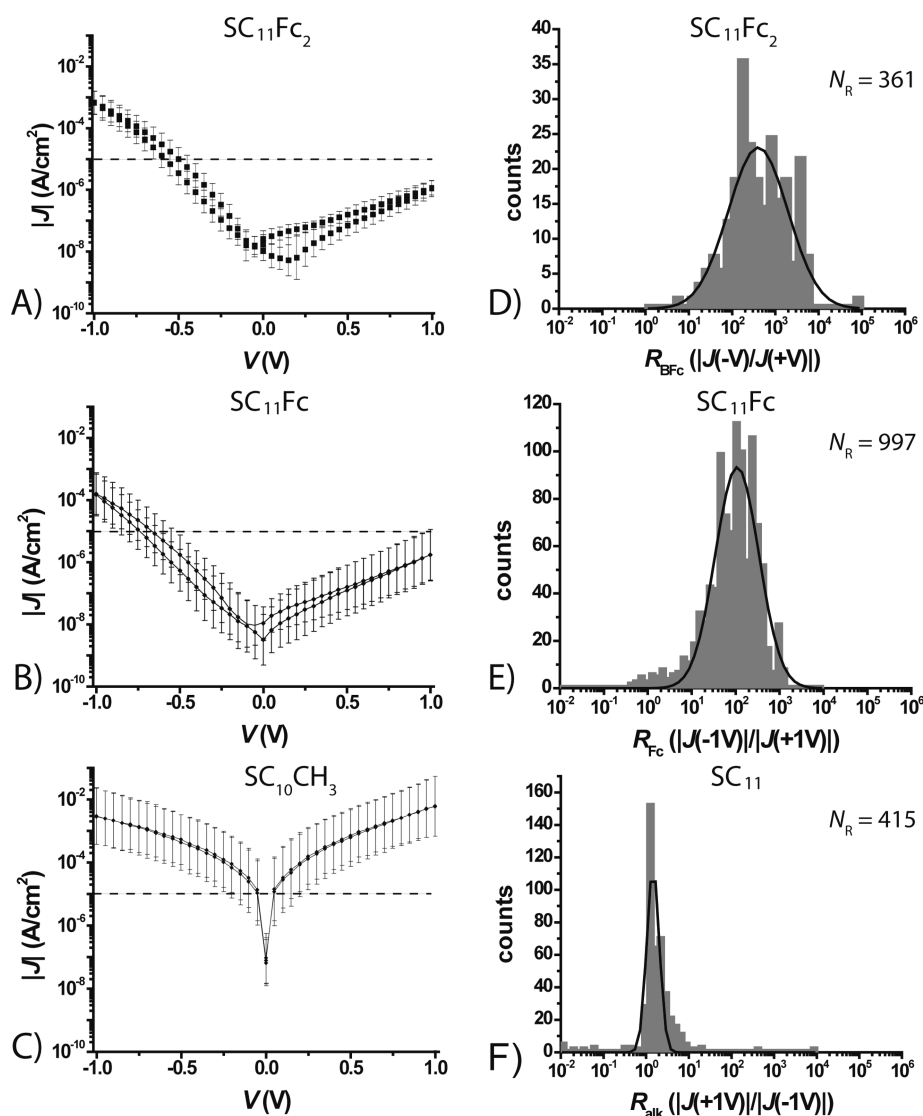


**Figure 3.** Log-average of the absolute current density  $|J|$  (A/cm<sup>2</sup>) plotted vs the voltage of the  $\text{Ag}^{\text{TS}}\text{-SC}_{11}\text{Fc}_2//\text{Ga}_2\text{O}_3/\text{EGaIn}$  junctions (25 junctions, 361 traces) (A),  $\text{Ag}^{\text{TS}}\text{-SC}_{11}\text{Fc}//\text{Ga}_2\text{O}_3/\text{EGaIn}$  junctions (53 junctions, 997 traces) (B), and  $\text{Ag}^{\text{TS}}\text{-SC}_{10}\text{CH}_3//\text{Ga}_2\text{O}_3/\text{EGaIn}$  junctions (23 junctions, 415 traces) (C). The error bars represent the log-standard deviation. The histograms with a Gaussian fit of the  $R$  of the  $\text{Ag}^{\text{TS}}\text{-SC}_{11}\text{Fc}_2//\text{Ga}_2\text{O}_3/\text{EGaIn}$  junctions (D),  $\text{Ag}^{\text{TS}}\text{-SC}_{11}\text{Fc}//\text{Ga}_2\text{O}_3/\text{EGaIn}$  junctions (E), and  $\text{Ag}^{\text{TS}}\text{-SC}_{10}\text{CH}_3//\text{Ga}_2\text{O}_3/\text{EGaIn}$  junctions (F) are also shown.  $N_R$  indicates the number of values of  $R$  measured for a particular type of junction. The width of the distribution of  $|J|$  for junctions with  $\text{C}_{10}\text{CH}_3$  is reproducible across many studies, and strongly suggests that the widths of the distributions of  $|J|$  for junctions with SAMs of  $\text{SC}_{11}\text{Fc}$  and  $\text{SC}_{11}\text{Fc}_2$  are due to (currently unidentified) features of the SAM, rather than the roughness of the  $\text{Ag}^{\text{TS}}$  surface, the  $\text{Ag}^{\text{TS}}\text{-SR}$  interface, or the  $\text{R}/\text{Ga}_2\text{O}_3/\text{EGaIn}$  interface.

$J(V)$  characteristics previously.<sup>1-3,32,51</sup> We developed a statistical procedure to measure the distribution of the values of  $J$ , to discriminate real data from artifacts, and to determine the yield of working devices and reproducibility.<sup>1,3,32</sup>

Figure 3 shows the  $|J(V)|$  curves (panels A–C) of the  $\text{Ag}^{\text{TS}}\text{-SC}_{11}\text{Fc}//\text{Ga}_2\text{O}_3/\text{EGaIn}$ ,  $\text{Ag}^{\text{TS}}\text{-SC}_{11}\text{Fc}_2//\text{Ga}_2\text{O}_3/\text{EGaIn}$ , and  $\text{Ag}^{\text{TS}}\text{-SC}_{10}\text{CH}_3//\text{Ga}_2\text{O}_3/\text{EGaIn}$  junctions, along with the histograms of the value of  $R$  obtained for each (panels D–F). Each point at a given voltage on the  $|J(V)|$  curve is the log-mean of all the (log-normally distributed) values of  $|J|$  measured at that voltage, and the error bars represent a factor of 1 log-standard deviation.

For each type of SAM, the Gaussian fit of  $\log(R)$  to the histogram yielded the log-mean ( $\mu_{\log}$ ) and log-standard deviation ( $\sigma_{\log}$ ), reported as  $R = \mu_{\log}(\sigma_{\log})$ . The  $\text{Ag}^{\text{TS}}\text{-SC}_{10}\text{CH}_3//\text{Ga}_2\text{O}_3/\text{EGaIn}$  junctions show only a small value of  $R = 1.7$  (1.35)

(Table 1). The higher values of currents appear at bias opposite to that for the  $\text{Ag}^{\text{TS}}\text{-SC}_{10}\text{CH}_3//\text{Ga}_2\text{O}_3/\text{EGaIn}$  and  $\text{Ag}^{\text{TS}}\text{-SC}_{11}\text{Fc}_2//\text{Ga}_2\text{O}_3/\text{EGaIn}$  junctions. A  $t$  test for significance indicated that the small rectification ratio observed at this junction is statistically different from unity.<sup>1</sup>

**Molecular Half-Wave Rectification of AC Potentials.** The large rectification ratios of the junctions based on Fc- and  $\text{Fc}_2$ -terminated SAMs make these attractive subjects for further investigation in simple circuits with AC signals (Figure 1).

Figure 4 shows the measured input voltage,  $V_{\text{in}}$  (black line), and the corresponding measured output voltage across the 1.5 M $\Omega$  resistor,  $V_{\text{out}}$  (red line), of circuits containing junctions of  $\text{Ag}^{\text{TS}}\text{-SC}_{10}\text{CH}_3//\text{Ga}_2\text{O}_3/\text{EGaIn}$  (Figure 4A),  $\text{Ag}^{\text{TS}}\text{-SC}_{11}\text{Fc}//\text{Ga}_2\text{O}_3/\text{EGaIn}$  (Figure 4B), and  $\text{Ag}^{\text{TS}}\text{-SC}_{11}\text{Fc}_2//\text{Ga}_2\text{O}_3/\text{EGaIn}$  (Figure 4C). The  $V_{\text{in}}$  was a 50 Hz sinusoidal signal with a peak



**Table 1. Statistics of the Ag<sup>TS</sup>-SAM//Ga<sub>2</sub>O<sub>3</sub>/EGaIn Junctions and Yields and Rectification Ratios**

type of SAM	total substrates <sup>a</sup>	total junctions <sup>b</sup>	total traces in histogram	short-circuit junctions	unstable junctions	yield <sup>c</sup> (%)	rectification ratio <sup>d</sup>
SC <sub>11</sub> Fc <sub>2</sub>	8	25	361	5 (20%)	3 (12%)	68	$5.0 \times 10^2$
SC <sub>11</sub> Fc	10	53	997	3 (5.6%)	4 (7.4%)	87	$1.0 \times 10^2$
SC <sub>10</sub> CH <sub>3</sub>	4	23	415	4 (17%)	3 (13%)	70	1.7

<sup>a</sup> We used 10 different template-stripped substrates from at least two wafers coated with 500 nm of Ag. <sup>b</sup> We formed the SAMs at the template-stripped Ag electrodes and contacted the SAMs with conically shaped electrodes of Ga<sub>2</sub>O<sub>3</sub>/EGaIn to complete the junctions. <sup>c</sup> We define a junction as “working” when its  $J(V)$  characteristics fall within three log-standard deviations from the mean value of  $J$ . <sup>d</sup> We determined these values of  $R$  by DC measurements at  $\pm 1.0$  V.

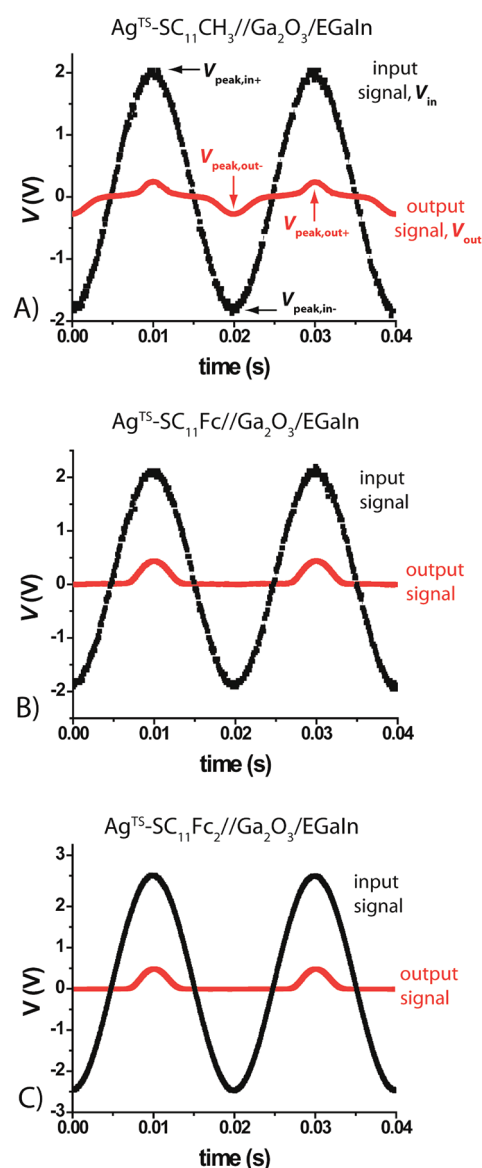
voltage,  $V_{\text{peak,in}}$  of 2.6 V for the Ag<sup>TS</sup>-SC<sub>11</sub>Fc<sub>2</sub>//Ga<sub>2</sub>O<sub>3</sub>/EGaIn junction and 2.1 V for the Ag<sup>TS</sup>-SC<sub>11</sub>Fc//Ga<sub>2</sub>O<sub>3</sub>/EGaIn and Ag<sup>TS</sup>-SC<sub>10</sub>CH<sub>3</sub>//Ga<sub>2</sub>O<sub>3</sub>/EGaIn junctions. The circuits containing SAMs with Fc or Fc<sub>2</sub> termini showed half-wave rectification (i.e., only the positive half of the sinusoidal input wave is present in the output signal), while the circuit containing the SAM of SC<sub>11</sub>CH<sub>3</sub> (and thus lacking the Fc or Fc<sub>2</sub> moieties) did not rectify. In all cases, the  $V_{\text{out}}$  signal is not detectably phase-shifted relative to  $V_{\text{in}}$ , but the values of  $V_{\text{out}}$  are significantly less than the values of  $V_{\text{in}}$  (see below).

The fact that the Ag<sup>TS</sup>-SC<sub>11</sub>Fc<sub>2</sub>//Ga<sub>2</sub>O<sub>3</sub>/EGaIn and Ag<sup>TS</sup>-SC<sub>11</sub>Fc//Ga<sub>2</sub>O<sub>3</sub>/EGaIn junctions function as half-wave rectifiers, while the Ag<sup>TS</sup>-SC<sub>10</sub>CH<sub>3</sub>//Ga<sub>2</sub>O<sub>3</sub>/EGaIn junctions do not, is in agreement with the  $J(V)$  curves shown in Figure 3. The Ag<sup>TS</sup>-SC<sub>10</sub>CH<sub>3</sub>//Ga<sub>2</sub>O<sub>3</sub>/EGaIn junctions have rectification ratios close to unity, while the Ag<sup>TS</sup>-SC<sub>11</sub>Fc<sub>2</sub>//Ga<sub>2</sub>O<sub>3</sub>/EGaIn and Ag<sup>TS</sup>-SC<sub>11</sub>Fc//Ga<sub>2</sub>O<sub>3</sub>/EGaIn junctions have rectification ratios of  $10^2$ – $10^3$  and, thus, are expected to behave like a diode.

**$J(V)$  Characteristics of the Diodes.** Solid-state diodes allow current to flow in one direct (at so-called forward bias) while blocking the current in the opposite direction (reverse bias). At forward bias, above a certain threshold voltage (the so-called turn-on voltage:  $\sim 0.7$  V for silicon-based p-n diodes),<sup>53</sup> the current increases exponentially with voltage. At reverse bias, only a small saturation current is observed until, at very large voltages ( $>75$  V), avalanche breakdown occurs and current flows. This large current normally leads to irreversible damage to the diode. A certain type of diode—the Zener diode—has a precisely controlled breakdown voltage, the so-called Zener voltage, at which current can flow without causing permanent damage to the diode (permanent damage to these diodes happens at much larger voltages). These diodes are used to control the voltage in a circuit.

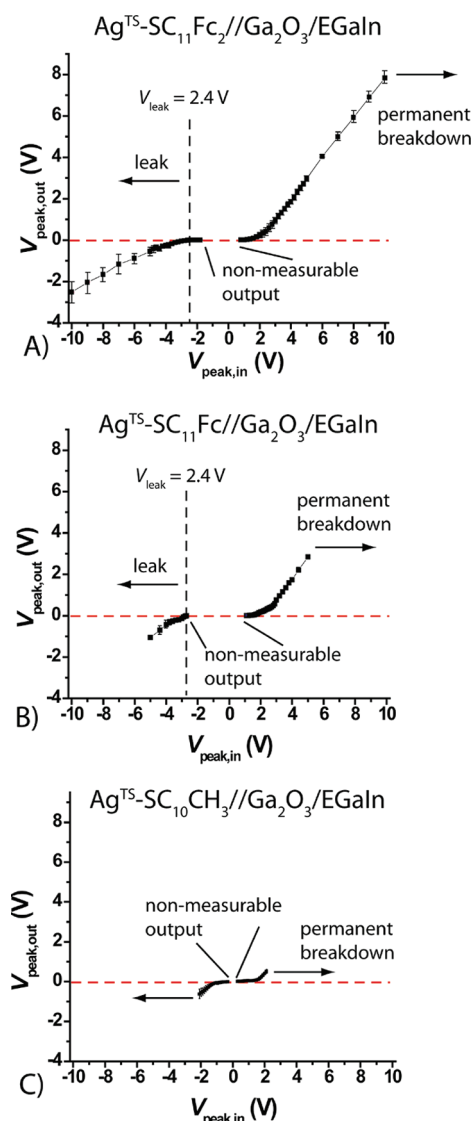
To study the behavior of the molecular diodes, we varied the peak voltage of the input signal,  $V_{\text{peak,in}}$  (V), and measured the peak voltage of the output signal,  $V_{\text{peak,out}}$  (V), across the resistor ( $1.5 \text{ M}\Omega$ ) as a function of time  $t$  (see below). Figure 5 shows a plot of  $V_{\text{peak,out}}$  as a function of  $V_{\text{peak,in}}$ . Figure 5 shows that the junctions composed of SAMs with Fc or Fc<sub>2</sub> termini have four important characteristics (summarized in Table 2) that we describe in the following sections. (i) At low values of  $V_{\text{peak,in}}$  ( $<0.8$  V),  $V_{\text{peak,out}}$  cannot be measured with the oscilloscope we used. (ii) At values of  $V_{\text{peak,in}}$  from 0.80 to 2.4 V, the diodes rectify. (iii) At values of  $V_{\text{peak,in}}$  greater than 2.4, the diodes leak current; that is, at negative voltages (or reversed bias), measurable values of  $V_{\text{peak,out}}$  are observed. (iv) At values of  $V_{\text{peak,in}}$  of 5–10 V, the diodes break down; that is, they short.

Figure 5 also shows that the  $V_{\text{peak,out}}$  at first increased nonlinearly with increasing  $V_{\text{peak,in}}$  but above a certain bias the response became linear. To explain this behavior, we discuss the



**Figure 4.** Sinusoidal input signals ( $V_{\text{in}}$ , black) with the corresponding output signal ( $V_{\text{out}}$ , red). These data are not smoothed; the noise levels of the data are in the mV range (see Figure 6 for examples). The input signal is sinusoidal (50 Hz), with a peak voltage ( $V_{\text{peak,in}}$ ) of 2.1 V for the Ag<sup>TS</sup>-SC<sub>10</sub>CH<sub>3</sub>//Ga<sub>2</sub>O<sub>3</sub>/EGaIn (A) and Ag<sup>TS</sup>-SC<sub>11</sub>Fc//Ga<sub>2</sub>O<sub>3</sub>/EGaIn junctions (B), and 2.6 V for the Ag<sup>TS</sup>-SC<sub>11</sub>Fc<sub>2</sub>//Ga<sub>2</sub>O<sub>3</sub>/EGaIn junctions (C).

peak voltage drop across the molecular junction ( $V_{\text{junction}}$ ). The junction and the resistor lie in series, and since the difference in



**Figure 5.**  $V_{\text{peak,out}}$  as a function of  $V_{\text{peak,in}}$  for the  $\text{Ag}^{\text{TS}}\text{-SC}_{11}\text{Fc}_2//\text{Ga}_2\text{O}_3/\text{EGaIn}$  (A),  $\text{Ag}^{\text{TS}}\text{-SC}_{11}\text{Fc}//\text{Ga}_2\text{O}_3/\text{EGaIn}$  (B), and  $\text{Ag}^{\text{TS}}\text{-SC}_{10}\text{CH}_3//\text{Ga}_2\text{O}_3/\text{EGaIn}$  junctions (C). Values of  $V_{\text{peak,in}} < 0.8$  V gave values of  $V_{\text{peak,out}}$  too small to be measurable with the oscilloscope. The devices rectified in the range  $1.0 \text{ V} < V_{\text{peak,in}} < 2.4$  V. Significant leakages could be observed for  $V_{\text{peak,in}} > 2.4$  V (see also Figure 7). See Supporting Information for an expanded view of panels B and C.

phase between  $V_{\text{in}}$  and  $V_{\text{out}}$  is negligible, Kirchhoff's circuit laws (eq 8)<sup>54</sup> dictate that the sum of the peak voltage drops across the junction and the resistor equals the peak input voltage:

$$V_{\text{junction}} = V_{\text{peak,in}} - V_{\text{peak,out}} \quad (8)$$

Figure 5 shows that at low values of  $V_{\text{peak,in}}$ , the values of  $V_{\text{peak,out}}$  are small and the values of  $V_{\text{junction}}$  approximately equal  $V_{\text{peak,in}}$ . This observation implies that the tunneling junctions are more resistive than the  $1.5 \text{ M}\Omega$  resistor at low bias. Consequently, the tunneling junction dominates the characteristics of the circuit and gives rise to the nonlinear regime in Figure 5. Conversely, at high values of  $V_{\text{peak,in}}$ , the voltage drop across the resistor meets and exceeds the voltage drop across the tunneling junction. In this regime, the ohmic characteristics of the resistor dominate the plot in Figure 5. The point of transition between

**Table 2.** Characteristics of the Molecular Junctions

SAM	$R$ (DC) <sup>a</sup>	$R$ (AC) <sup>b</sup>	$V_{\text{leak}}$ (V) <sup>c</sup>	$V_{\text{break}}$ (V) <sup>d</sup>	molecular length (nm) <sup>e</sup>
$\text{SC}_{11}\text{Fc}_2$	$5.0 \times 10^2$	$2.0 \times 10^2$	$2.4 \pm 0.1$	$-5.0 \pm 0.5$	2.8
$\text{SC}_{11}\text{Fc}$	$1.0 \times 10^2$	$2.0 \times 10^2$	$2.7 \pm 0.1$	$-4.1 \pm 0.2$	2.1
$\text{SC}_{10}\text{CH}_3$	1.7	$\sim 2$	—	$-1.5 \pm 0.2$	1.3

<sup>a</sup> Measured at  $\pm 1.0$  V using  $J(V)$  curves obtained using DC (Figure 2).

<sup>b</sup> Measured at  $\pm 2.0$  V using the data obtained with AC (Figure 5).

<sup>c</sup> Input voltage at which leakage current is observed. <sup>d</sup> Effective potential drops across the junctions (see text for details). <sup>e</sup> Estimated from CPK models.

the nonlinear and linear regions in Figure 5 denotes the bias at which the voltage drop (and the resistance) across the tunneling junction is approximately equal to that across the resistor. As expected, the voltage drop across the junctions decreased by replacing the  $1.5 \text{ M}\Omega$  resistor by a resistor of  $15 \text{ M}\Omega$ , while substituting a  $150 \text{ k}\Omega$  resistor had the opposite effect and also resulted in shorts at much lower input voltages of  $< 6.0$  V (see Supporting Information) than those junctions in circuits with the two large resistors.

**Leak Voltage.** Figure 6 shows  $V_{\text{out}}$  (the entire waveform) as a function of time  $t$  for three different values of  $V_{\text{peak,in}} \leq V_{\text{leak}}$  in circuits incorporating tunneling junctions based on SAMs of  $\text{SC}_{11}\text{Fc}$ ,  $\text{SC}_{11}\text{Fc}_2$ , and  $\text{SC}_{10}\text{CH}_3$ .

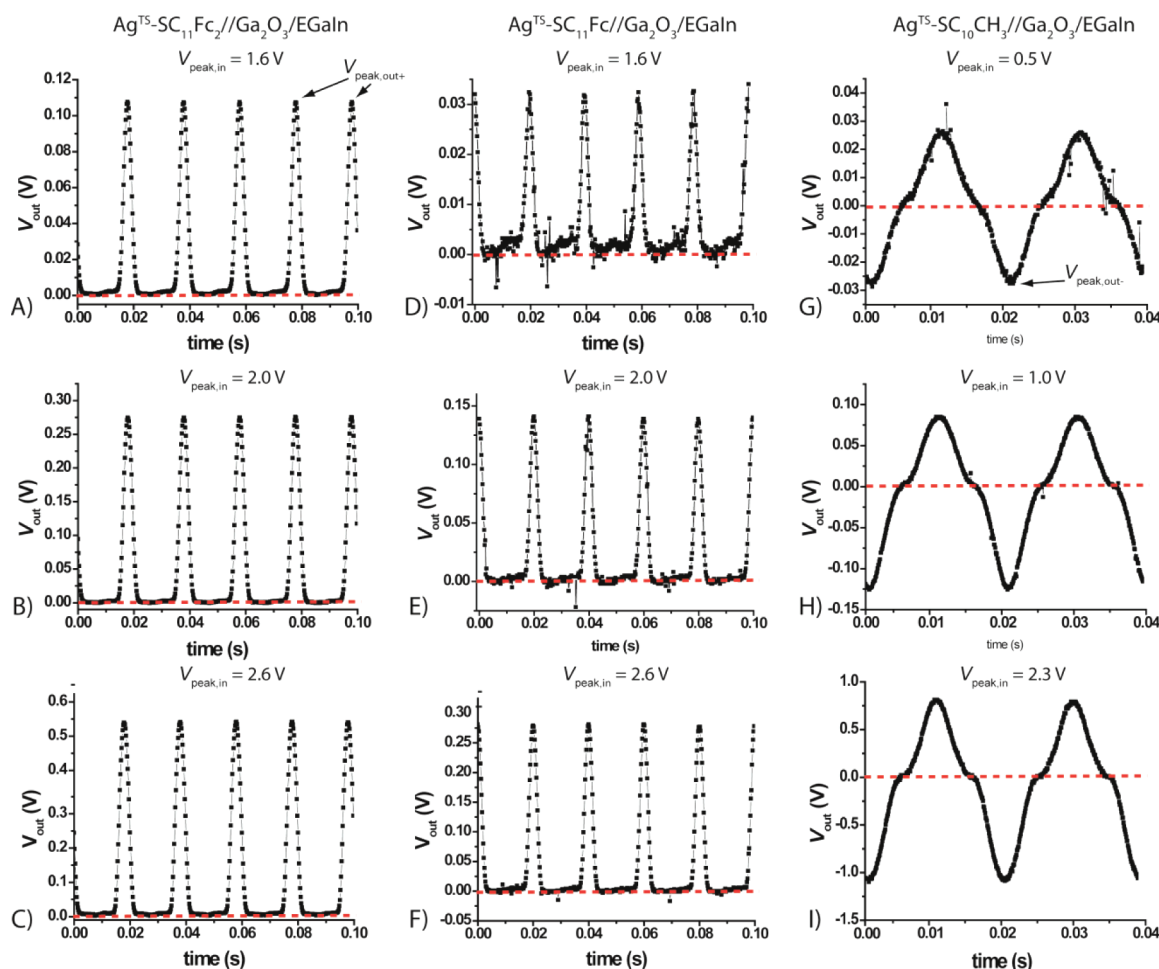
For junctions having the structure  $\text{Ag}^{\text{TS}}\text{-SC}_{11}\text{Fc}//\text{Ga}_2\text{O}_3/\text{EGaIn}$  and  $\text{Ag}^{\text{TS}}\text{-SC}_{11}\text{Fc}_2//\text{Ga}_2\text{O}_3/\text{EGaIn}$ , the oscilloscope detected very small to no output at reverse bias (i.e., low leakage,  $|V| < 0.005$  V) for values of  $V_{\text{peak,in}} < 2.4$  V. At  $V_{\text{peak,in}} \approx V_{\text{leak}} = 2.4$  V, the  $V_{\text{peak,out}}$  at forward bias for the  $\text{Ag}^{\text{TS}}\text{-SC}_{11}\text{Fc}//\text{Ga}_2\text{O}_3/\text{EGaIn}$  junctions was  $0.31 \pm 0.10$  V (or 13% of the value of  $V_{\text{peak,in}}$ ) and that of the  $\text{Ag}^{\text{TS}}\text{-SC}_{11}\text{Fc}_2//\text{Ga}_2\text{O}_3/\text{EGaIn}$  junctions was  $0.42 \pm 0.18$  V (or 18% of the value of  $V_{\text{peak,in}}$ ). These results imply rectification ratios of  $R > 100$ ; this estimate agrees with that obtained with DC measurements (Table 2). Although the junctions composed of  $\text{Fc}_2$  SAMs perform better than the junctions composed of  $\text{Fc}$  SAMs, the  $V_{\text{peak,out}}$  is less than  $\sim 20\%$  of the  $V_{\text{peak,in}}$  when  $V_{\text{peak,in}} \approx V_{\text{leak}}$ . Thus, the junctions behave as half-wave rectifiers, but they have large internal resistances.

Figure 7 shows  $V_{\text{out}}$  as a function of time  $t$  for two different values of  $V_{\text{peak,in}} > V_{\text{leak}}$  of circuits composed of tunneling junctions of SAMs of  $\text{SC}_{11}\text{Fc}$  ( $V_{\text{peak,in}} = 3.0$  or  $5.0$  V) and  $\text{SC}_{11}\text{Fc}_2$  ( $V_{\text{peak,in}} = 5.0$  or  $10.0$  V). At values for  $V_{\text{peak,in}} > 2.4$  V, the oscilloscope could measure leakage at reverse bias (Table 2). For  $V_{\text{peak,in}} \approx V_{\text{break}} = 5.0$  V, the value of  $V_{\text{peak,out}} = 2.84 \pm 0.04$  V for  $\text{Ag}^{\text{TS}}\text{-SC}_{11}\text{Fc}_2//\text{Ga}_2\text{O}_3/\text{EGaIn}$  junction was 57% of the value of the input signal, but the rectification ratio dropped to 5. For the  $\text{Ag}^{\text{TS}}\text{-SC}_{11}\text{Fc}_2//\text{Ga}_2\text{O}_3/\text{EGaIn}$  junctions, for  $V_{\text{peak,in}} = 10.0$  V, the value of  $V_{\text{peak,out}} = 7.8 \pm 0.3$  V was about 78% of the input signal, but the rectification ratio was only 1.6 (we have not tested this value statistically to determine whether it is distinguishable from  $R = 1$ , or no rectification).

Reducing  $V_{\text{peak,in}}$  to below the value of  $V_{\text{leak}}$  restored half-wave rectification; thus, the processes that let the molecular diode pass current at reverse bias, and eliminate rectification, are reversible, and do not permanently damage these molecular diodes.

The sharp decrease in rectification ratio at biases above  $2.4$  V and the large decrease of the internal resistance of the tunneling junction clearly imply a change in the mechanisms of charge





**Figure 6.**  $V_{\text{out}}$  as a function of time for the  $\text{Ag}^{\text{TS}}\text{-SC}_{11}\text{Fc}_2//\text{Ga}_2\text{O}_3/\text{EGaIn}$  (A–C),  $\text{Ag}^{\text{TS}}\text{-SC}_{11}\text{Fc}//\text{Ga}_2\text{O}_3/\text{EGaIn}$  (D–F), and  $\text{Ag}^{\text{TS}}\text{-SC}_{10}\text{CH}_3//\text{Ga}_2\text{O}_3/\text{EGaIn}$  (G–I) junctions with three different values of  $V_{\text{in}}$ . The red dashed line indicates  $V_{\text{out}} = 0.0$  V.

transport in going from low bias voltage to high bias voltage (see below).

#### Determination of the Mechanisms of Charge Transport.

To investigate the mechanisms of charge transport in the tunneling junctions, we determined the  $I(V)$  characteristics of the junction. We report  $I(V)$  curves rather than  $J(V)$  curves for the AC measurements because we do not know the effective area of the resistor we used in our circuits. Equation 9 describes the voltage across the junction in the circuit summarized in Figure 1. Kirchhoff's circuit laws<sup>54</sup> further dictate that, since the tunneling junction and the resistor lie in series, and since  $V_{\text{in}}$  and  $V_{\text{out}}$  are approximately equal in phase, the current flowing through the junction,  $I_{\text{junction}}$ , equals the current flowing through the resistor. The latter is given by Ohm's law as voltage divided by resistance (eq 9).

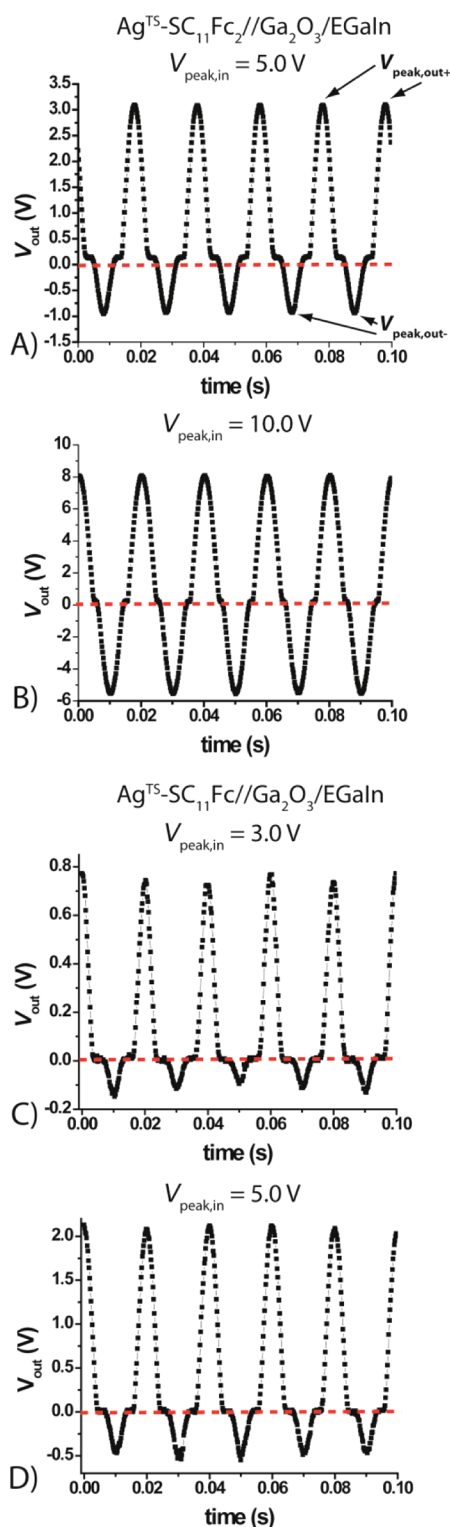
$$I_{\text{junction}} = \frac{V_{\text{peak,out}}}{R} \quad (9)$$

Note that  $I_{\text{junction}}$  is the total peak current through the molecular junction, including both tunneling current and possible capacitive current due to the close proximity of the  $\text{Ga}_2\text{O}_3/\text{EGaIn}$  and Ag electrodes. Although the capacitive contribution to the current could be determined by frequency-dependent measurements, we have not attempted to separate these two contributions due to the limitations of our simple apparatus at high frequencies.

Instead, we used a frequency of 50 Hz and assumed that at this low frequency any capacitive contributions were not important.

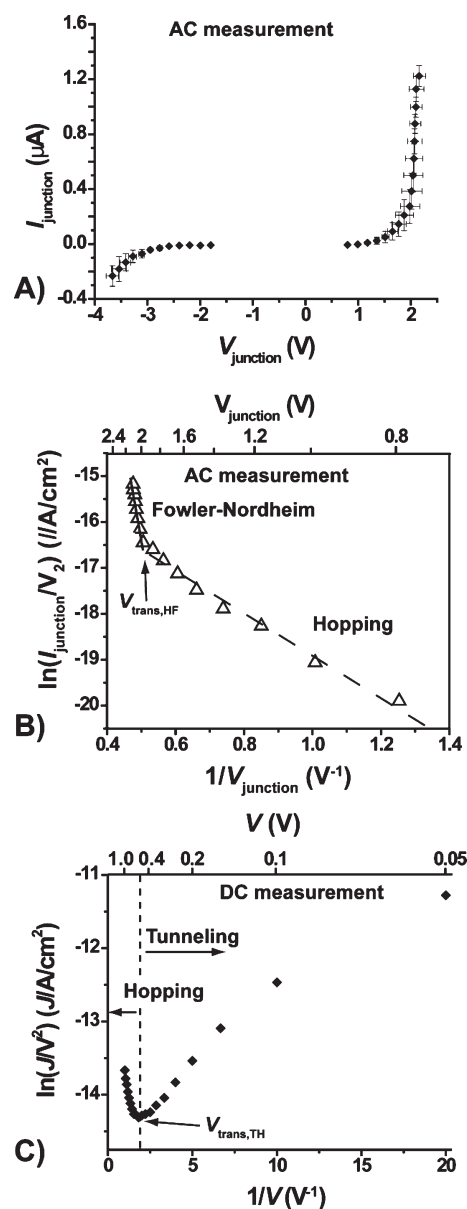
To construct  $I(V)$  curves for the junctions, we determine  $I_{\text{junction}}$  and  $V_{\text{junction}}$  with eqs 8 and 9. Figure 8A shows the  $I(V)$  curve obtained for the  $\text{Ag}^{\text{TS}}\text{-SC}_{11}\text{Fc}_2//\text{Ga}_2\text{O}_3/\text{EGaIn}$  junctions over the range  $-4.0 < V_{\text{junction}} < 2.0$  V.  $V_{\text{junction}}$  did not exceed these limits, even at extreme values of  $V_{\text{peak,in}}$  ( $\pm 10$  V), because, at these values of  $V_{\text{junction}}$ , the SAM is relatively conductive, and any increase in  $V_{\text{peak,in}}$  manifests itself as an increased potential drop across the resistor, rather than the SAM. While  $V_{\text{junction}}$  remains roughly constant at large values of  $V_{\text{peak,in}}$ ,  $I_{\text{junction}}$  still increases linearly with increasing input voltage. The  $I(V)$  curve of the molecular diode near the extreme values of  $V_{\text{junction}} = -4.0$  and 2.0 V is, therefore, unreliable and has a large error. The region of the  $I(V)$  curve between  $-1.7 \text{ V} < V_{\text{junction}} < 0.7 \text{ V}$  was not accurately measurable due to the insensitivity of the oscilloscope. Figure 3, however, shows the  $J(V)$  curve for the bias range of  $\pm 1.0$  V obtained by DC experiments. Thus, Figures 8A and 3A show the electrical characteristics over the entire bias regime from  $-4.0$  to 2.0 V.

Figure 8B shows a plot of  $\ln(I/V^2)$  vs  $1/V$ , i.e., a FN plot, of the same data shown in Figure 8A for  $\text{Ag}^{\text{TS}}\text{-SC}_{11}\text{Fc}_2//\text{Ga}_2\text{O}_3/\text{EGaIn}$  junctions at positive bias. Figure 8C shows the FN plot for the data obtained in DC experiments (Figure 3A). These plots show three characteristics. The FN plots (Figure 8B,C) show (i) a clear transition from logarithmic growth to linear



**Figure 7.**  $V_{\text{out}}$  as a function of time using a sinusoidal input signal with amplitudes of 5.0 (A) and 10.0 V (B) for the  $\text{Ag}^{\text{TS}}\text{-SC}_{11}\text{Fc}_2//\text{Ga}_2\text{O}_3/\text{EGaIn}$  junctions, and 3.0 (C) and 5.0 V (D) for the  $\text{Ag}^{\text{TS}}\text{-SC}_{11}\text{Fc}/\text{Ga}_2\text{O}_3/\text{EGaIn}$  junctions.

decay (Figure 8C), (ii) a cusp (i.e., a point where the tangent to the curve abruptly changes slope) in the region of logarithmic growth (Figure 8B), and (iii) that this cusp is observed only at positive bias, and not at negative bias.



**Figure 8.** (A) Plot of current through the SAM ( $I_{\text{junction}}$ ) vs voltage across the SAM ( $V_{\text{junction}}$ ) averaged over six junctions of  $\text{Ag}^{\text{TS}}\text{-SC}_{11}\text{Fc}_2//\text{Ga}_2\text{O}_3/\text{EGaIn}$ . The text describes the procedure for calculating  $I_{\text{junction}}$  and  $V_{\text{junction}}$ . (B) Plot of  $\ln(|I/V_{\text{junction}}^2|)$  vs  $1/V_{\text{junction}}$  for the  $\text{Ag}^{\text{TS}}\text{-SC}_{11}\text{Fc}_2//\text{Ga}_2\text{O}_3/\text{EGaIn}$  junction at positive bias. The solid black line is a least-squares fit to eq 6 and indicates the region with FN tunneling as the dominant mechanism of charge transport. The dashed black line is a guide to the eyes and indicates the region with hopping as the dominant mechanism of charge transport. (C) Plot of  $\ln(|I/V_{\text{junction}}^2|)$  vs  $1/V_{\text{junction}}$  for the  $\text{Ag}^{\text{TS}}\text{-SC}_{11}\text{Fc}_2//\text{Ga}_2\text{O}_3/\text{EGaIn}$  junction, using the data obtained by DC methods (Figure 3). The dashed line indicates  $V_{\text{trans,TH}} = 0.50$  V, the transition from tunneling to hopping.

We first discuss the mechanisms of charge transport at positive bias. At low bias of  $<0.50$  V, the FN plot indicates that tunneling is the dominant mechanism of charge transport. In this regime of voltage,  $J(V)$  measurements as a function of temperature indicate that indeed tunneling is the dominant mechanism of charge transport.<sup>32</sup> At voltages in the range over 0.50–1.9 V, the FN plot shows a linear increase, and the slope of this line changes at 1.9 V,

resulting in a cusp (Table 3). We showed for junctions of  $\text{Ag}^{\text{TS}}\text{-SC}_{11}\text{Fc}/\text{Ga}_2\text{O}_3/\text{EGaIn}$  (by  $J(V)$  measurements as a function of temperature using DC methods) that hopping is the dominant mechanism of charge transport in the bias range of 0.50–1.0 V.<sup>32</sup> We did not observe hopping at opposite bias. For this bias range, FN tunneling, which has negligible temperature dependence, is excluded as a possible mechanism. We believe that the mechanism of charge transport changes from tunneling to hopping at  $V = 0.50$  V and call this transition “the transition voltage from tunneling to hopping”, or  $V_{\text{trans,TH}}$ . We believe that the increase in the slope in the FN plot (Figure 8C) at  $V = 1.9$  V indicates a transition in the mechanism of charge transport from hopping to FN tunneling, and we call this transition “the transition voltage from hopping to FN tunneling”, or  $V_{\text{trans,HF}}$ . Thus, the interpretation of FN plots requires caution, because a minimum in a FN plot does not necessarily indicate a change in the mechanism of charge transport from tunneling to FN tunneling.

**Table 3. Different Types of Transition Voltages for the  $\text{Ag}^{\text{TS}}\text{-SAM}/\text{Ga}_2\text{O}_3/\text{EGaIn}$  Junctions**

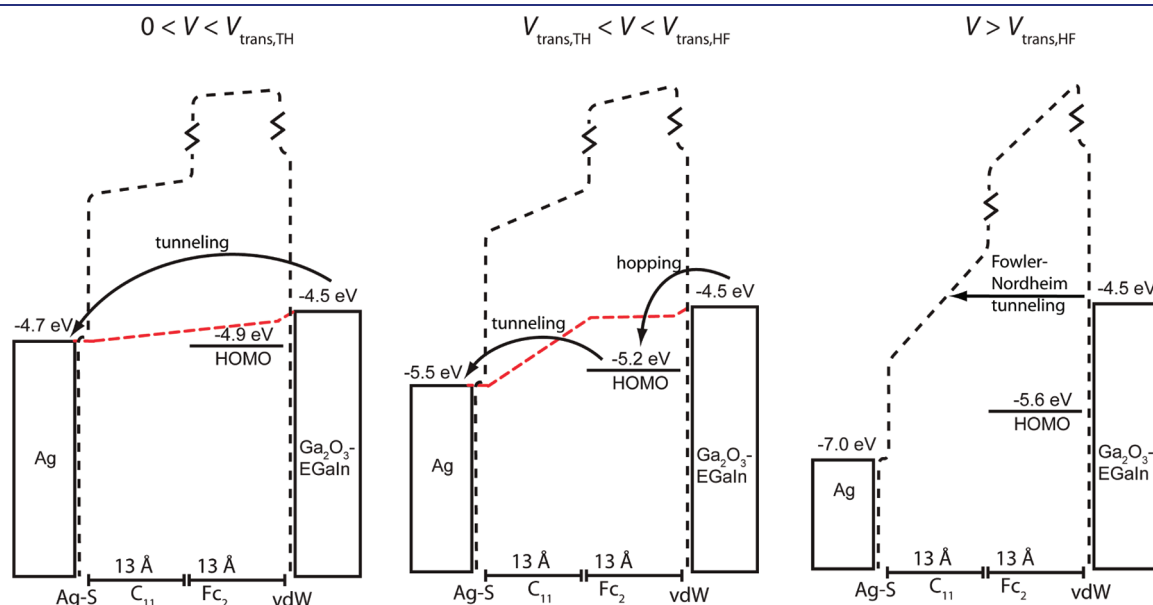
SAM	$V_{\text{trans,TH}}$ (V) <sup>a</sup>	$V_{\text{trans,HF}}$ (V) <sup>c</sup>
$\text{SC}_{10}\text{CH}_3$	— <sup>b</sup>	1.3
$\text{SC}_{11}\text{Fc}$	0.50	2.1
$\text{SC}_{11}\text{Fc}_2$	0.50	1.9

<sup>a</sup>  $V_{\text{trans,TH}}$  is the transition voltage at which we observed the transition in the mechanism of charge transport from tunneling to hopping. <sup>b</sup> Temperature-dependent measurements indicated that hopping does not occur across these SAMs. <sup>c</sup>  $V_{\text{trans,HF}}$  is the transition voltage at which we observed the transition in the mechanism of charge transport from hopping to FN tunneling.

The mechanism of charge transport at positive bias is different from that at negative bias. The FN plot for negative bias also shows a transition in the mechanism of charge transport. We believe that this transition indicates a change in the mechanism of charge transport from tunneling (at biases less than  $-0.50$  V) to FN tunneling (at biases greater than  $-0.50$  V). The FN plot for large negative bias obtained with the AC experiments does not show a change in the slope of the graph, or cusp. Thus, the mechanism of charge transport is consistent with FN tunneling over the entire bias regime of  $-0.50$  to  $-4.0$  V.

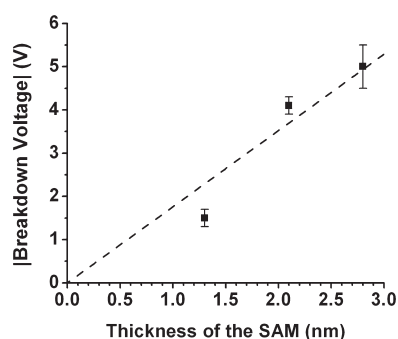
Our findings agree with our earlier finding that the rectification by the SAMs with Fc termini is caused by the fact that hopping is the dominant mechanism of charge transport in one direction of bias, and not in the other (Figure 2).<sup>32</sup> But here we show that, at voltages larger than  $V_{\text{trans,HF}}$ , FN tunneling is the dominant mechanism of charge transport in both directions of bias and causes rectification to diminish to a value close to unity (see below). Junctions with SAMs of  $\text{SC}_{11}\text{Fc}$  and  $\text{SC}_{11}\text{Fc}_2$  behave in the same way, but with slightly different values of  $V_{\text{trans,HF}}$  (Table 3). Tables 2 and 3 show that  $V_{\text{leak}}$  is nearly the same as  $V_{\text{trans,HF}}$ . Thus, these molecular junctions start to leak current shortly after the mechanism of charge transport changes from hopping to FN tunneling.

Figure 9 shows the three energy-level diagrams of the junctions of  $\text{Ag}^{\text{TS}}\text{-SC}_{11}\text{Fc}_2/\text{Ga}_2\text{O}_3/\text{EGaIn}$  for open circuit, and at applied biases  $V = -1.0$ ,  $-2.4$ , or  $-3.4$  V, and summarizes the mechanisms of charge transport across these junctions in the three different potential ranges of  $0 \text{ V} < V_{\text{trans,TH}}$ ,  $V_{\text{trans,TH}} < V < V_{\text{trans,HF}}$ , and  $V > V_{\text{trans,HF}}$ . The potentials drops across these junctions have been described in ref 3 and are briefly described in the Prior Work section. At a bias of less than 0.5 V, or lower than  $V_{\text{trans,TH}}$ , these measurements indicated that tunneling across the



**Figure 9.** Schematic representations of the proposed energy level diagrams for  $\text{Ag}^{\text{TS}}\text{-SC}_{11}\text{Fc}_2/\text{Ga}_2\text{O}_3/\text{EGaIn}$  junctions for the applied voltages  $V$  in the range of  $0 < V < V_{\text{trans,TH}}$  when tunneling dominates ( $V = 0.2$  V; left), in the range of  $V_{\text{trans,TH}} < V < V_{\text{trans,HF}}$  when hopping dominates ( $V = 1.0$  V; middle), and in the range of  $V > V_{\text{trans,HF}}$  ( $V = 2.5$  V; right) when FN tunneling dominates the mechanism of charge transport. As in Figure 2, the black dotted lines qualitatively show that the LUMO levels of the alkyl chain ( $-2.6$  to  $-2.9$  eV)<sup>37</sup> and the  $\text{Fc}_2$  moiety ( $\sim -0.4$  eV)<sup>38,39</sup> across the junction were greater for negative bias than for positive bias. Since the positive peak voltage across the rectifying junctions was roughly independent of  $V_{\text{peak,in}}$  at large bias, we suspect that irreversible breakdown occurs under negative applied bias. We therefore define the irreversible breakdown voltage as the peak negative voltage across the junction when breakdown occurs (Table 2). Figure 10 shows the irreversible breakdown voltage as a function of the thickness of the monolayer  $d$ . The electric field  $E$  between two parallel plates depends on the applied voltage  $V$  and the distance  $d$  between the two plates (eq 10).





**Figure 10.** Linear dependence of the irreversible breakdown voltage on the thickness of the SAMs ( $\text{SC}_{11}$ ,  $\text{SC}_{11}\text{Fc}$ , and  $\text{SC}_{11}\text{Fc}_2$ , from left to right). Breakdown occurred at negative bias for all SAMs. The dotted line shows a linear fit, constrained to pass through the origin, of the three points. The slope of this fit represents the approximate field required to achieve breakdown. The error bars represent the standard deviation of six measurements.

whole SAMs is the dominant mechanism of charge transport, and that the molecular diodes do not rectify ( $R \approx 1-5$ ). At a bias of  $V_{\text{trans,TH}} < |V| < V_{\text{trans,HF}}$ , the dominant mechanism of charge transport is hopping in only the direction of bias (here negative), and the molecular diodes have their maximal rectification ratios ( $R > 100$ ).<sup>3,32</sup> At biases of  $|V| > V_{\text{trans,HF}}$ , FN tunneling is the dominant mechanism of charge transport, and the molecular diodes do not rectify ( $R \approx 1-5$ ).

**Breakdown Voltage.** To test the robustness of the molecular diodes, we increased  $V_{\text{peak,in}}$  until the output signal changed irreversibly. Irreversible breakdown indicated a short across the molecular junction, and resulted in  $V_{\text{in}} = V_{\text{out}}$  (the same result observed for an  $\text{Ga}_2\text{O}_3/\text{EGaIn}$  tip contacting a bare  $\text{Ag}^{\text{TS}}$  substrate lacking a SAM).

In DC experiments,<sup>1,3</sup> the voltage of breakdown for the  $\text{Ag}^{\text{TS}}\text{-SC}_{11}\text{Fc}_2//\text{Ga}_2\text{O}_3/\text{EGaIn}$  junctions was approximately 1.5 V. In these experiments, the voltage dropped almost entirely across the junction because a resistor in series with the junction is not present.

In our AC experiments (Figure 1), the voltage of breakdown in our tunneling junctions was much higher (Table 2). We report the voltage of breakdown in terms of the actual voltage drop across the junction at negative bias, not the input voltage ( $V_{\text{peak,in}}$ ), which drops across both the junction and the resistor. At large values of  $V_{\text{peak,in}}$ , the junctions were damaged permanently and the circuits shorted; the corresponding peak voltage across the junction was greater for negative bias than for positive bias. Since the positive peak voltage across the rectifying junctions was roughly independent of  $V_{\text{peak,in}}$  at large bias, we suspect that irreversible breakdown occurs under negative applied bias. We therefore define the irreversible breakdown voltage as the peak negative voltage across the junction when breakdown occurs (Table 1). Figure 10 shows the irreversible breakdown voltage as a function of the thickness of the monolayer,  $d$ . The electric field  $E$  between two parallel plates depends on the applied voltage  $V$  and the distance  $d$  between the two plates (eq 10).

$$E = V/d \quad (10)$$

Here, we assume the distance between the two electrodes to be defined by the thickness of the SAM (that is, we neglect other contributions to contact resistance). We calculated the thicknesses of the SAMs according to the following assumptions: (i) the C–C bond length in the alkyl chain is 1.54 Å, (ii) the S–C

bond length is 1.8 Å, (iii) the angle between bonds in the alkyl chain is 104.5°, and (iv) the diameter of the Fc moiety is 6.7 Å. According to eq 10, for a given applied voltage, thicker SAMs experience weaker electric fields between electrodes than do thinner SAMs and are, therefore, less prone to breakdown.<sup>55</sup> The slope of the linear fit of the plot in Figure 9 approximates the field required to achieve breakdown in these junctions as  $(1.8 \pm 0.2) \times 10^9$  V/m. Following eq 10, the linear fit was artificially constrained to pass through the origin.

Our experiment indicates that the thickness of the SAM is the primary factor that determines the breakdown voltage: the thicker the SAM, the higher the value of the breakdown voltage. These findings are in agreement with a much more comprehensive study concerning the breakdown field involving a large number of SAMs of different chemical structures.<sup>55</sup> This study concluded that the breakdown field is  $\sim 0.8 \times 10^9$  V/m, is insensitive to the chemical structure of the SAM, and is primarily determined by the thickness of the SAM inside the junction.<sup>55</sup> The values for the breakdown voltage and field we determined using AC methods are about a factor of 2 larger than the values obtained by DC methods.<sup>55</sup> We believe that this difference in breakdown fields (and voltages) indicates that using an AC signal does, indeed, minimize the formation of, for instance, metal filaments inside the junctions.<sup>30,29</sup>

**Rectification Ratio Determined by Half-Wave Rectification.** Normally, we determine the value of  $R$  by DC measurements using eq 1. The rectification ratio can also be determined when the molecular diodes are operating as half-wave rectifiers. In this type of experiment, the ratio of the peak potential at positive bias ( $V_{\text{peak,out+}}$ ) to the peak potential at negative bias ( $V_{\text{peak,out-}}$ ) at the output gives the rectification ratio as described by eq 11.

$$R = V_{\text{peak,out+}}/V_{\text{peak,out-}} \quad (11)$$

Figure 6 shows the output characteristics of the diodes. Thus, at biases greater than  $V_{\text{leak}}$ , the rectification ratio can be determined by simply dividing the peak positive potential of the output signal by the peak negative potential. At biases less than  $V_{\text{leak}}$ , the output signals are too small to be detectable by the simple oscilloscope we used in this study, and  $R$  could not be determined reliably using this method. We determined the values of  $R$  reliably using DC experiments; Figure 3 shows that the rectification ratios at a bias of  $\pm 1$  V are  $> 10^2$ . Figure S2 shows the  $J(V)$  curves obtained with DC measurement for a  $\text{Ag}^{\text{TS}}\text{-SC}_{11}\text{Fc}_2//\text{Ga}_2\text{O}_3/\text{EGaIn}$  junction measured at potentials up to 2.0 V ( $< 5\%$  of the junctions withstood this bias range; none of the  $\text{Ag}^{\text{TS}}\text{-SC}_{11}\text{Fc}_2//\text{Ga}_2\text{O}_3/\text{EGaIn}$  junctions could withstand potentials larger than  $\pm 1.5$  V). Figure S2 shows that this junction rectified maximally up to 2.0 V ( $R \approx 1.0 \times 10^3 - 1.2 \times 10^3$ , measured at  $\pm 2.0$  V), indicating consistency between AC and DC measurements with respect to rectification.

The rectification ratio is not constant and depends on the  $V_{\text{peak,in}}$  (Figures 6–8). Figure 11 shows the  $R$  of the  $\text{Ag}^{\text{TS}}\text{-SC}_{11}\text{Fc}_2//\text{Ga}_2\text{O}_3/\text{EGaIn}$  junctions as a function of  $V_{\text{peak,in}}$ . Figure 11 shows that, at biases less than  $V_{\text{leak}}$ ,  $R$  cannot be determined reliably using eq 11. The tunneling junctions still rectified in this bias regime, even though  $R$  could not be quantified. Hopping, at negative bias, and field emission, at positive bias, dominate the mechanism of charge transport. At biases greater than  $V_{\text{leak}}$ , Figure 11 shows that  $R$  drops close to unity. Thus, as concluded earlier, in this bias regime the tunneling

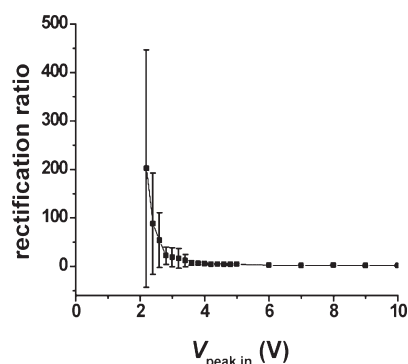


**Figure 11.** Rectification ratio of the Ag<sup>TS</sup>-SC<sub>11</sub>Fc<sub>2</sub>//Ga<sub>2</sub>O<sub>3</sub>/EGaIn junctions determined as the ratio of  $V_{\text{peak,out+}}$  and  $V_{\text{peak,out-}}$  as a function of  $V_{\text{peak,in}}$ .

junctions are not rectifying, and the mechanism of charge transport is dominated by field emission in both directions of bias.

## CONCLUSIONS

### Molecular Diodes Can Operate as Half-Wave Rectifiers.

The method described in this paper to study the mechanism of charge transport across SAM-based junctions makes it possible to study the performance of molecular diodes in real circuitry—here circuits in which they replaced a conventional diode—and requires only a wave generator and an oscilloscope. We used AC signals of 50 Hz with amplitudes ranging from 0.8 to 10.0 V, and showed that these molecular diodes can operate as half-wave rectifiers. The properties of these molecular diodes (with form Ag<sup>TS</sup>-SC<sub>11</sub>Fc<sub>*m*</sub>//Ga<sub>2</sub>O<sub>3</sub>/EGaIn; *m* = 1 or 2) are different from those of classic diodes. These molecular diodes behave as half-wave rectifiers up to a voltage across the junction of  $\sim 1.9$  V, above which the rectification ratio decreases almost to unity, i.e., no rectification. Lowering the voltage to below this value restored rectification. At voltages of 5.0 V, or higher for the thickest SAM in this study of SC<sub>11</sub>Fc<sub>2</sub>, the molecular diodes tend to break down by shorting. These molecular diodes rectified for 30–40 min with sinusoidal signals (with an amplitude of 2.0–3.0 V, 50 Hz), that is,  $>10^5$  cycles.

**The Breakdown Voltage in AC Experiments Is Larger than in DC Experiments.** The breakdown voltage of the junctions of  $1.8 \pm 0.2$  GV/m determined by this AC method is about a factor of 2 larger than that determined by DC methods.<sup>55</sup> This difference in breakdown voltage might indicate that, during AC measurements, the formations of metal filaments, and possibly other processes leading to failure, are minimized. These processes are slower than the time scale of the experiment (20 ms at a frequency of 50 Hz), at least, and perhaps to some extent reversible.<sup>30,29</sup> Thus, using this AC method makes it possible to study charge-transfer processes across SAM-based junctions over a much wider potential range than using DC methods.

The mechanism of charge transport changes as a function of applied bias and involves tunneling, hopping, and FN tunneling. Using this method, we identified three different types of charge transport. (i) At biases across the junctions in the range of 0–0.5 V, tunneling dominates the mechanism of charge transport, and the molecular diodes do not rectify ( $R \approx 1$ –5). (ii) At biases in the range of 0.5–2.4 V, hopping dominates the mechanism of charge transport in one direction of bias, and

tunneling in the other, and the molecular diodes have their maximum rectification ratios ( $R > 100$ ). (iii) At biases above 2.4 V, and up to the breakdown voltage, FN tunneling dominates the mechanism of charge transport, and the molecular diodes do not rectify ( $R \approx 1$ –5).

**The Interpretation of Fowler–Nordheim Plots without Temperature-Dependent Data Might Be Ambiguous.** In large electric fields ( $\sim$ GV/m), the mechanism of charge transport can change from tunneling to FN tunneling (that is, to electron emission from the metal electrodes to the SAM under the influence of large electric fields). Normally, observation of a minimum in a so-called FN plot (Figure 8) at a particular bias ( $V_{\text{trans}}$ ) indicates a transition in the mechanism of charge transport from tunneling to field emission (FN tunneling). We showed that care is needed in the interpretation of FN plots: the observation of  $V_{\text{trans}}$  does not necessarily mean that the mechanism of charge transport changes from tunneling to field emission. We observed a minimum in these plots (at  $V = 0.50$  V; Figure 8C), but temperature-dependent measurements ruled out the transition from tunneling to field emission (both are independent of temperature) at this bias, and indicated a transition from tunneling to hopping (which is dependent on the temperature). We observed a change in the mechanism of charge transport from hopping to FN tunneling that resulted in a cusp in the FN plot at  $V \approx 1.9$  V (Figure 8B). Without temperature-dependent measurements, thus, interpretation of FN plots might be ambiguous because the observation of  $V_{\text{trans}}$  might indicate the transition from tunneling to hopping rather than the transition from tunneling to FN tunneling.

**Our Molecular Diodes Do Not Meet the Standards of Commercial Diodes.** Normally molecular diodes are discussed only in terms of rectification ratios determined in DC experiments: molecular diodes with high values of  $R$  are better than those with low values of  $R$ . The terms “high” and “low” are not well-defined, but values of  $R > 10$  are considered to be high in most studies of organic rectifiers.<sup>6,10,13,56</sup> Many studies report values of  $R < 10$ ,<sup>7,9,16,17</sup> although these values are so close to unity (i.e., not rectifying) that their statistical significance must be rigorously demonstrated, using sufficient sample sizes and statistical tests, before they can be considered rectifying. Commercially available conventional diodes, however, fulfill many specifications depending on the specific applications.<sup>53</sup> Here we identify four characteristics that are important to all types of commercial diodes. (i) The rectification ratio must be large (in a typical p–n diode,  $R$  increases exponentially with voltage, beyond a certain “turn-on voltage”, and can reach values of  $10^4$ – $10^8$ ). (ii) The internal resistance at forward bias must be low (typically  $<10 \Omega$  at the turn-on voltage, and even lower at higher bias), while the current at reverse bias (saturation current) must also be minimal (typically  $<10^{-5}$  A). (iii) The lifetime must be long (years). (iv) The operational bias window, outside of which the diode breaks down, must be large ( $|V| > 50$ – $70$  V, although for specific applications smaller bias windows are acceptable).

Our molecular diodes do not fulfill any of these four requirements. (i) The rectification ratios are too low, although the values we report for our molecular rectifier are the largest reported to date for an interpretable, statistically validated SAM-based system. (ii) The resistance in forward bias is too large (in the order of  $10^6 \Omega$ ) when operating under conditions with the largest values of  $R$  ( $\geq 100$ ). (iii) The lifetimes are too short (30–40 min in operation). (iv) The bias window (maximum value of  $\pm 5$  V for junctions of Ag<sup>TS</sup>-SC<sub>11</sub>Fc<sub>2</sub>//Ga<sub>2</sub>O<sub>3</sub>/EGaIn) at

which the diodes can operate is too small. Thus, to identify “good” molecular diodes only by comparison of the rectification ratios with other organic thin films is not sufficient to conclude or imply that these molecular diodes have any potential for practical use as rectifiers.

**Inherent Limitations of Molecular Diodes.** We identified two inherent limitations of our molecular diodes, which may apply to any other molecular diode. (i) The molecular diodes change the mechanism of charge transport from hopping (in one direction of bias) and tunneling (in the other direction of bias) to FN tunneling (in both directions of bias) for values of  $V_{in} > V_{TF} \approx 2.4$  V, at which voltage the values of  $R$  decreased to values of close to unity, i.e., no rectification. In this bias regime, the mechanism of charge transport is not determined by the chemical structure of the SAMs. Thus, the performances of molecular diodes are limited by the transition from any type of charge transport to FN tunneling at large input biases. (ii) The molecular diodes break down (probably by shorting) in a field of 1.8 GV/m; this field seems to be independent of the chemical structure of the SAM. Thus, molecular diodes of even the size of large (5 nm) molecules will break down at an input voltage exceeding  $\sim 10$  V (or 2 GV/m).

## ■ ASSOCIATED CONTENT

**S Supporting Information.** Experimental procedures, nomenclature, expansion of Figure 5, and the  $J(V)$  characteristics (DC measurement) of a  $Ag^{TS}-SC_{11}Fc_2//Ga_2O_3/EGaIn$  junction that was stable during  $J(V)$  measurement of  $\pm 2.0$  V. This material is available free of charge via the Internet at <http://pubs.acs.org>.

## ■ AUTHOR INFORMATION

### Corresponding Author

[gwhitesides@gmwhgroup.harvard.edu](mailto:gwhitesides@gmwhgroup.harvard.edu); [christian.nijhuis@nus.edu.sg](mailto:christian.nijhuis@nus.edu.sg)

## ■ ACKNOWLEDGMENT

C.A.N. acknowledges The Netherlands Organization for Scientific Research (NWO) for the Rubicon grant supporting this research and the Singapore National Research Foundation under NRF Award No. NRF-RF2010-03. Research was supported by the U.S. Department of Energy, Office of Basic Energy Sciences, Division of Materials Sciences and Engineering, under Award No. DE-FG02-00ER45852 (AC measurements and apparatus), and by the National Science Foundation under Award No. CHE-05180055 (synthesis of materials and support for W.F.R.). A.C.S. acknowledges the Howard Hughes Medical Institute and the Harvard-MIT Division of Health Science and Technology for fellowship support.

## ■ REFERENCES

- (1) Nijhuis, C. A.; Reus, W. F.; Whitesides, G. M. *J. Am. Chem. Soc.* **2009**, *131*, 17816.
- (2) Chiechi, R. C.; Weiss, E. A.; Dickey, M. D.; Whitesides, G. M. *Angew. Chem., Int. Ed.* **2008**, *47*, 142.
- (3) Nijhuis, C. A.; Reus, W. F.; Whitesides, G. M. *J. Am. Chem. Soc.* **2010**, *132*, 18386.
- (4) In the circuit shown in Figure 1, the polarity of the rectifier is reversed with respect to the current density measurements, in which the electrodes were arranged such that the junctions passed current selectively at negative voltage, rather than positive voltage. For our demonstration of a half-wave rectifier, we have switched the polarity of the electrodes to conform to the convention of the community; that is, the current is allowed to pass at positive voltage.
- (5) Aviram, A.; Ratner, M. A. *Chem. Phys. Lett.* **1974**, *29*, 277.
- (6) Metzger, R. M. *Acc. Chem. Res.* **1999**, *32*, 950.
- (7) Shumate, W. J.; Mattern, D. L.; Jaiswal, A.; Dixon, D. A.; White, T. R.; Burgess, J.; Honciuc, A.; Metzger, R. M. *J. Phys. Chem. B* **2006**, *110*, 11146.
- (8) Ashwell, G. J.; Ewinton, J.; Robinson, B. J. *Chem. Commun.* **2006**, 618.
- (9) Ng, M.-K.; Lee, D.-C.; Yu, L. *J. Am. Chem. Soc.* **2002**, *124*, 11862.
- (10) Peterson, I. R.; Vuillaume, D.; Metzger, R. M. *J. Phys. Chem. A* **2001**, *105*, 4702.
- (11) Lenfant, S.; Krzeminski, C.; Delerue, C.; Allan, G.; Vuillaume, D. *Nano Lett.* **2003**, *3*, 741.
- (12) Chabiny, M. L.; Chen, X.; Holmlin, R. E.; Jacobs, H.; Skulason, H.; Frisbie, C. D.; Mujica, V.; Ratner, M. A.; Rampi, M. A.; Whitesides, G. M. *J. Am. Chem. Soc.* **2002**, *124*, 11730.
- (13) Ashwell, G. J.; Urasinska-Wojcik, B.; Phillips, L. J. *Angew. Chem., Int. Ed.* **2010**, *49*, 3508.
- (14) Gayathri, S. S.; Patnaik, A. *Chem. Commun.* **2006**, 1977.
- (15) Honciuc, A.; Jaiswal, A.; Gong, A.; Ashworth, K.; Spangler, C. W.; Peterson, I. R.; Dalton, L. R.; Metzger, R. M. *J. Phys. Chem. B* **2005**, *109*, 857.
- (16) Chen, X.; Jeon, Y.-M.; Jang, J.-W.; Qin, L.; Huo, F.; Wei, W.; Mirkin, C. A. *J. Am. Chem. Soc.* **2008**, *130*, 8166.
- (17) Böhme, T.; Simpson, C. D.; Müllen, K.; Rabe, J. P. *Chem.—Eur. J.* **2007**, *13*, 7349.
- (18) Chen, X.; Jeon, Y.-M.; Jang, J.-W.; Qin, L.; Huo, F.; Wei, W.; Mirkin, C. A. *J. Am. Chem. Soc.* **2008**, *130*, 8166.
- (19) Metzger, R. M.; Chen, B.; HoIpfner, U.; Lakshmikantham, M. V.; Vuillaume, D.; Kawai, T.; Wu, X.; Tachibana, H.; Hughes, T. V.; Sakurai, H.; Baldwin, J. W.; Hosch, C.; Cava, M. P.; Brehmer, L.; Ashwell, G. J. *J. Am. Chem. Soc.* **1997**, *119*, 10455.
- (20) Salomon, A.; Boecking, T.; Chan, C. K.; Amy, F.; Girshevitz, O.; Cahen, D.; Kahn, A. *Phys. Rev. Lett.* **2005**, *95*, 266807.
- (21) Salomon, A.; Boecking, T.; Seitz, O.; Markus, T.; Amy, F.; Chan, C.; Zhao, W.; Cahen, D.; Kahn, A. *Adv. Mater.* **2007**, *19*, 445.
- (22) Salomon, A.; Böcking, T.; Gooding, J. J.; Cahen, D. *Nano Lett.* **2006**, *6*, 2873.
- (23) Bang, G. S.; Chang, H.; Koo, J.-R.; Lee, T.; Advincula, R. C.; Lee, H. *Small* **2008**, *4*, 1399.
- (24) Kim, T.-W.; Wang, G.; Lee, H.; Lee, T. *Nanotechnology* **2007**, *18*, 315204.
- (25) Lau, C. N.; Stewart, D. R.; Williams, R. S.; Bockrath, M. *Nano Lett.* **2004**, *4*, 569.
- (26) Bebee, J. M.; Kushmerick, J. G. *Appl. Phys. Lett.* **2007**, *90*, 083117.
- (27) Walker, A. V.; Tighe, T. B.; Cabarcos, O. M.; Reinard, M. D.; Haynie, B. C.; Uppili, S.; Winograd, N.; Allara, D. L. *J. Am. Chem. Soc.* **2004**, *126*, 3954.
- (28) We are preparing a manuscript that collects this evidence in one place, and provides additional evidence that we believe conclusively demonstrates the molecular origin of rectification in our diodes. Reus, W. F.; Thuo, M. M.; Nijhuis, C. A.; Shapiro, N.; Whitesides, G. M., unpublished material.
- (29) Pierce, D. G.; Brusius, P. G. *Microelectron. Reliab.* **1997**, *37*, 1053.
- (30) Krumbein, S. J. *IEEE Trans. Compds., Hybrids, Manuf. Technol.* **1988**, *11*, 5.
- (31) McCreery, R. L. *Chem. Mater.* **2004**, *16*, 4477.
- (32) Nijhuis, C. A.; Reus, W. F.; Barber, J.; Dickey, M. D.; Whitesides, G. M. *Nano Lett.* **2010**, *10*, 3611.
- (33) Barr, T. L.; Seal, S. J. *Vac. Sci. Technol. A* **1995**, *13*, 1239.
- (34) Cademartiri, L.; Thuo, M. M.; Nijhuis, C. A.; Barber, J. R.; Sodhi, R. N. S.; Brodersen, P.; Kim, C.; Reus, W. F.; Chiechi, R. C.; Whitesides, G. M., unpublished results.
- (35) Reus, W. F.; Nijhuis, C. A.; Barber, J.; Thuo, M. M.; Cademartiri, L.; Kim, C.; York, R. L.; Liu, X.; Whitesides, G. M., unpublished results.



- (36) Lorenz, M. R.; Woods, J. F.; Gambino, R. J. *J. Phys. Chem. Solids* **1967**, *28*, 403.
- (37) Li, C. P.; Wei, K. H.; Huang, J. Y. *Angew. Chem., Int. Ed.* **2006**, *45*, 1449.
- (38) Kitagawa, K.; Morita, T.; Kimura, S. *J. Phys. Chem. B* **2005**, *109*, 13906.
- (39) Tivanski, A. V.; Walker, G. C. *J. Am. Chem. Soc.* **2005**, *127*, 7647.
- (40) Müller-Meskamp, L.; Karthäuser, S.; Zandvliet, H. J. W.; Homberger, M.; Simon, U.; Waser, R. *Small* **2009**, *5*, 496.
- (41) Liu, Y.; Offenhäusser, A.; Mayar, D. *Phys. Status Solidi A* **2010**, *207*, 891.
- (42) Choi, S. H.; Kim, B. S.; Frisbie, C. F. *Science* **2008**, *320*, 1482.
- (43) Beebe, J. M.; Kim, B.; Gadzuk, J. W.; Frisbie, D. C.; Kushmerick, J. G. *Phys. Rev. Lett.* **2006**, *97*, 026801.
- (44) Beebe, J. M.; Kim, B. S.; Frisbie, D. C.; Kushmerick, J. G. *ACS Nano* **2008**, *2*, 827.
- (45) Engelkes, V. B.; Beebe, J. M.; Frisbie, C. D. *J. Am. Chem. Soc.* **2004**, *126*, 14287.
- (46) Lindsay, S. M.; Ratner, M. A. *Adv. Mater.* **2007**, *19*, 23.
- (47) Simmons, J. G. *J. Appl. Phys.* **1963**, *34*, 1793.
- (48) Simmons, J. G. *J. Appl. Phys.* **1963**, *34*, 2581.
- (49) McConnell, H. M. *J. Chem. Phys.* **1961**, *508*, 515.
- (50) Joachim, C.; Ratner, M. A. *Proc. Natl. Acad. Sci. U.S.A.* **2005**, *102*, 8801.
- (51) Weiss, E. A.; Chiechi, R. C.; Kaufman, G. K.; Kriebel, J. K.; Li, Z.; Duati, M.; Rampi, M. A.; Whitesides, G. M. *J. Am. Chem. Soc.* **2007**, *129*, 4336.
- (52) Love, J. C.; Estroff, L. A.; Kriebel, J. K.; Nuzzo, R. G.; Whitesides, G. M. *Chem. Rev.* **2005**, *105*, 1103.
- (53) Dorf, R. C., Ed. *The Electrical Engineering Handbook*; CRC Press: Boca Raton, FL, 1993.
- (54) Paul, C. R. *Fundamentals of Electric Circuit Analysis*; John Wiley & Sons: New York, 2001.
- (55) Haag, R.; Rampi, M. A.; Holmlin, R. E.; Whitesides, G. M. *J. Am. Chem. Soc.* **1999**, *121*, 7895.
- (56) McCreery, R. L.; Bergren, A. J. *Adv. Mater.* **2009**, *21*, 4303.